AFCRC-TN-56-259

TURBULENT DIFFUSION OF MOMENTUM AND HEAT FROM A SMOOTH, PLANE BOUNDARY WITH ZERO PRESSURE GRADIENT

By

A. C. Spengos

Department of Civil Engineering

Scientific Report No. 1

The research reported in this document has been sponsored by the Geophysics Research Directorate of the Air Force Cambridge Research Center, Air Research and Development Command, under Contract AF19(604)-421.

Colorado Agricultural and Mechanical College

Fort Collins, Colorado

FEBRUARY, 1956

CER No. 56ACS 4

ABSTRACT

Results of an experimental investigation of the turbulent diffusion of momentum and heat from a smooth, plane boundary with zero pressure gradient are presented. A 10 ft long, 6 ft wide heated boundary maintained at a uniform temperature, formed part of the floor of the 6-ft square test section of a recirculating, low velocity wind tunnel.

The velocities have been measured with hot-wire anemometers and the Reynolds stress distribution in the boundary layer has been computed from the measurements of the crossed-hot-wire anemometers. The temperatures have been measured with thermocouples, and the transferred heat has been determined from the electrical input to the heated boundary. Data on the pertinent variables have been collected along the centerline of the boundary and at four cross-sections of the boundary layer.

The distribution of the mean velocity, for both neutral stability and various lapse rates, was found to be described more accurately by a "modified logarithmic law" The distribution of the mean temperature in the thermal boundary layer was found to be similar to that of the mean velocity when momentum and thermal boundary layers are of the same thickness. The local drag coefficient was found to increase considerably with increasing negative Richardson numbers. Also Karman's modification of the Reynolds analogy between momentum and heat transfer was found to be in good agreement with the experimental results.

CONTENTS

ABSTRACT i

ACKNOWLEDGMENTS v

LIST OF SYMBOLS vii

SYMBOLS USED IN FIGURES FOR NEUTRAL STABILITY xi

SYMBOLS USED IN FIGURES FOR HEATED BOUNDARY xii

I. INTRODUCTION 1

II. EXPERIMENTAL EQUIPMENT AND PROCEDURE 3

Wind Tunnel 3
Heated Boundary 3
Velocity Measurements 4
Shear Stress Measurements 5
Temperature Measurements 5
Heat Input Measurements 6
Collection of Data 6

III. DISCUSSION OF RESULTS 7

The Mean Velocity Profile 7
The Mean Temperature Profile 10
The Local Drag Coefficient and the Distribution of Shear 11
The Eddy Diffusivity 14
The Relation Between Momentum and Heat Transfer 16
Miscellaneous Remarks 18

IV. SUMMARY OF RESULTS 19

REFERENCES 21

FIGURES 23

ACKNOWLEDGMENTS

The experimental study herein presented was made possible through the financial support of the Air Force Cambridge Research Center under Contract No. AF 19(604)-421. The constructive assistance of Dr. H. Lettau, contract monitor representing the Air Force Cambridge Research Center, is gratefully appreciated.

Many thanks are due to all of the fluid mechanics staff members of the Civil Engineering Department of Colorado A and M College for contributions during the progress of this study. In particular, acknowledgments are made to Dr. M. L. Albertson, Head of Fluid Mechanics Research for suggesting the study and for general advice, to Prof. J. E. Cermak for preliminary planning and designing of the experimental equipment, to Dr. P. N. Lin for his contributions in the analysis of the data, to Mr. R. W. Sjostrom for his valuable assistance in the instrumentation phase of the study and in collecting the data, to Prof. H. H. Schweizer for designing part of the apparatus, and to Mr. R. T. Shen for his meticulous care in editing this report.

The work reported herein was conducted in the low-velocity wind tunnel of the Civil Engineering Department of Colorado A and M College. Acknowledgment is made to Prof. T. H. Evans, Dean of Engineering and Dr. D. F. Peterson, Head of the Department of Civil Engineering for their support and assistance.

LIST OF SYMBOLS

c_p	specific heat of air at constant pressure
g	gravitational acceleration
k	Karman constant -- $\frac{2.3\ U_*}{U_1 - U_{0.1}}$
n	exponent
q_o	heat transferred per unit area and unit time
$\overline{uv}$	Reynolds stress
u'	root-mean-square value of the fluctuating component of the local velocity in the direction of u
v'	root-mean-square value of the fluctuating component of the local velocity in the direction of v
x	distance downstream from the beginning of the heated boundary
x'	distance downstream from the beginning of the test section
z	distance measured vertically from the surface of the heated boundary
A	heated boundary area upstream from the point where measurements were taken
C_e	vapor transfer coefficient -- $\frac{E}{\rho g U_o \Delta C}$
C_f	local drag coefficient
C_H	heat transfer coefficient -- $\frac{q_o}{\rho U_o c_p \Delta T}$
ΔC	change in water vapor concentration
E	evaporation weight per unit area and unit time
K	thermal conductivity of air -- $\frac{\mu_m c_p}{Pr}$
K_t	thermal diffusivity of air -- $\frac{\nu_m}{Pr}$
N	evaporation coefficient -- $\frac{E\ x}{\Delta C\ \nu_e}$
Nu	Nusselt number -- $\frac{Q_o\ x}{K\ A\ \Delta T}$

LIST OF SYMBOLS.--Continued

Pe	Peclet number -- $\frac{U_* x}{K_t}$
Pr	Prandtl number -- $\frac{\mu c_p}{K}$
Qo	total amount of heat transferred from heated boundary upstream from the point where measurements were taken
R_*	Reynolds number -- $\frac{U_* x}{\nu_e}$
$R_{x'}$	Reynolds number -- $\frac{U_o x'}{\nu}$
Ri	Richardson number -- $\frac{g \left(\frac{dT}{dz}\right)}{(T_a)_{abs} \left(\frac{dU}{dz}\right)^2}$
Ri_δ	Richardson number -- $\frac{g \frac{\Delta T}{\delta_t}}{(T_a)_{abs} (U_o/\delta)^2}$
Ri_x	Richardson number -- $\frac{g \Delta T x}{(T_a)_{abs} U_o^2}$
$R_{x'm}$	Reynolds number -- $\frac{U_o x'}{\nu_m}$
St	Stanton number -- $\frac{Nu}{Pe}$
T	local mean temperature -- °F
T_a	ambient mean temperature -- °F
$(T_a)_{abs}$	ambient mean temperature -- °K
T_s	mean temperature at the surface of the heated boundary
ΔT	$(T_a - T_s)$
U	x-component of the velocity of mean motion
U_*	mean shear velocity on the surface of the heated boundary -- $U_o\sqrt{\frac{C_f}{2}}$

U_i correction term for the modified logarithmic velocity distribution -- $\frac{U_*}{k} \ln \left[\frac{3\,(2 - z/\delta\,)}{1 + 5\,(1 - z/\delta\,)^{1.5}} \right]$

U_1 mean velocity 1 in. from the surface

$U_{0.1}$ mean velocity 0.1 in. from the surface

U_o mean ambient velocity

δ thickness of the momentum boundary layer (value of z for $0.99\ U_o$ velocity change)

δ_t thickness of the thermal boundary layer (value of z for $0.99\ \Delta T$)

ϵ eddy diffusivity

η Reynolds number -- $\frac{z\,U_*}{\nu}$

η_m Reynolds number -- $\frac{z\,U_*}{\nu_m}$

θ dimensionless mean temperature -- $\frac{(T - T_s)}{(T_a - T_s)}$

μ dynamic viscosity of air

μ_m mean dynamic viscosity of air in the thermal boundary layer

ν kinematic viscosity of air

ν_m mean kinematic viscosity of air in the thermal boundary layer

ν_e molecular diffusivity coefficient for water vapor into air

ρ_m mean density of air in the thermal boundary layer

σ Prandtl number -- $\frac{\nu}{\nu_e}$

τ shearing stress in the direction of x

SYMBOLS USED IN FIGURES
FOR NEUTRAL STABILITY.

Symbol	U_o fps	x' ft	x ft	δ in.
	10.0	5.3	0.29	1.70
	10.0	6.0	0.96	1.90
	10.0	8.3	3.29	2.30
	10.0	14.3	9.30	3.00
	14.0	5.3	0.29	1.80
	14.0	6.0	0.96	1.90
	14.0	8.3	3.29	3.30
	14.0	14.3	9.30	4.20
	17.0	5.3	0.29	1.60
	17.0	6.0	0.96	1.80
	17.0	8.3	3.29	2.50
	17.0	14.3	9.30	2.80
	35.0	5.3	0.29	1.60
	35.0	6.0	0.96	1.90
	35.0	8.3	3.29	2.40
	35.0	14.3	9.30	4.00

SYMBOLS USED IN FIGURES
FOR HEATED BOUNDARY.

Symbol	U_o fps	x' ft	x ft	T_a °F	ΔT °F	δ in.	δ_t in.
	10.0	5.3	0.29	70.0	118.0	1.80	0.60
	10.0	6.0	0.96	74.0	115.0	2.00	1.30
	10.0	8.3	3.29	75.0	106.0	2.20	2.30
	10.0	14.3	9.30	72.0	99.0	2.80	4.00
	14.0	5.3	0.29	34.0	73.0	1.65	0.60
	14.0	6.0	0.96	41.0	69.0	1.85	1.00
	14.0	8.3	3.29	40.0	62.0	2.75	2.50
	14.0	14.3	9.30	40.0	58.0	3.20	4.20
	17.0	5.3	0.29	50.0	93.0	1.80	0.45
	17.0	6.0	0.96	51.0	85.0	2.20	0.95
	17.0	8.3	3.29	52.0	82.0	2.50	2.00
	17.0	14.3	9.30	50.0	77.0	3.80	4.00
	35.0	5.3	0.29	64.0	62.0	1.60	0.30
	35.0	6.0	0.96	67.0	60.0	1.80	0.70
	35.0	8.3	3.29	63.0	59.0	2.50	1.70
	35.0	14.3	9.30	60.0	56.0	4.00	4.00

I. INTRODUCTION

The transfer of momentum, heat, vapor, and sediment by turbulent diffusion is one of the problems in fluid dynamics which has attracted considerable attention during the last forty or fifty years. By observing the diurnal variations of the lower atmosphere, the evaporation from free surfaces, or the sediment transportation by rivers, one realizes that this is an interminable process in nature and of paramount importance to scientists such as meteorologists, agronomists, oceanographers and engineers.

Efforts to understand this complex phenomenon of transfer have led to several important hypotheses explaining the nature of its mechanism. The following are those that have received considerable attention. The hypothesis of the exchange coefficients, proposed by Boussinesq and developed by Wilhelm Schmidt, is based on the fundamental ideas of the kinetic theory of gases. Prandtl's mixing length and Karman's similarity hypotheses also have their origin in the kinetic theory of gases. Sutton's theory of turbulent exchange may be regarded as an application of the theory of diffusion by continuous movements proposed by Taylor in 1920. In the particular case of heat transfer, Reynolds' analogy between fluid friction and heat transfer has been extended by Karman in the light of the results of modern turbulence research on velocity distribution near solid boundaries.

The results presented in this report constitute the first part of the experimental investigation of the turbulent diffusion of momentum and heat from a smooth, plane boundary with zero pressure gradient. The boundary was heated electrically in such a way that its entire surface could be set at uniform temperature thus affording experimental conditions for two-dimensional flow of air, and heat transfer. Various lapse rates, as indicated by Richardson number, were obtained from the variation of the ambient velocity and the surface temperature of the boundary.

For momentum transfer, the data were analyzed using the exchange coefficient hypothesis, while for heat transfer, Sutton's (16) turbulent exchange theory and Cermak's (1) equation, based on Reynolds' analogy as modified by Karman (6), were used for theoretical comparison. Also, Reichardt's (12) suggestion for the modification of the logarithmic law of the velocity distribution was applied to flow over smooth boundaries under both neutral stability and lapse rate conditions. Profiles of the pertinent variables for various lapse rates are also presented.

As it is frequently the case with experimental investigations, the results presented herein indicate the need for extending the experimental range and further developing and improving the instrumentation and equipment involved.

II. EXPERIMENTAL EQUIPMENT AND PROCEDURE

The equipment for the experimental study consisted of a recirculating wind tunnel, a smooth, plane, boundary heated electrically to a uniform temperature over its entire surface, and the instrumentation for the measurement of the pertinent variables.

Wind Tunnel

The recirculating tunnel has a 6-ft square test section 30 ft in length. A plan of the tunnel is shown in Fig. 1. Preliminary tests indicated that the amount of heat transferred from the heated boundary did not appreciably affect the ambient air temperature; consequently, it was decided to recirculate the air. However, with minor alterations, the tunnel could be operated as a non-recirculating type if necessary.

The range of the velocities attainable in the test section was from 3 fps to 50 fps. The distribution of the ambient velocity, both along the centerline of the test section and perpendicular to it, did not vary more than 2% from the mean value. Also, the pressure variation along the centerline was of the same order of magnitude. The turbulence level of the ambient air stream was approximately 1% for 17 fps mean velocity.

Heated Boundary

The dynamically smooth and heated boundary, over which the momentum and thermal boundary layers developed, was 6 ft wide, 10 ft long, and formed part of the floor of the test section. It consisted of a 1/2-in. aluminum plate on top of which the heater strips, covering the entire surface, were mounted. Figure 2 shows the location of the heated boundary in the test section. Proper adjustment of the electrical input to each strip made possible the realization of a surface of uniform temperature. These strips, comprising the 23 electrically isolated heating elements, consisted of 1/16-in. aluminum supporting plates, of varying width, on which a thin layer of carbon was placed. The top and bottom of the carbon layer were electrically insulated by several layers of varnish. In Fig. 3 the construction details of the heated boundary are shown. Under the 1/2-in. aluminum plate a 4-in. layer of glass wool provided adequate thermal insulation. Measurements have shown that only 2% of the heat input was dissipated from surfaces other than the top over which the thermal boundary layer developed.

The temperature of the boundary was set with the aid of a movable thermocouple in direct contact with the surface and by individual adjustment of the current through each strip. The variation of the temperature over the entire surface was within 6°F of the desired temperature along the centerline of the boundary.

To stimulate the development of the turbulent boundary layer a $1\frac{1}{2}$-ft strip of 1/8-in. gravel was laid across the floor of the test section and ahead of the heated boundary as shown in Fig. 2. In Fig. 4 the points of inception of the momentum and thermal boundary layers are shown diagramatically.

Velocity Measurements

The mean velocity profiles as well as the ambient velocity were measured with a platinum hot-wire anemometer 0.4 in. long and 0.001 in. in diameter. The velocity measuring element formed one branch of a manually balanced Wheatstone bridge and it was compensated for changes in the ambient temperature by a resistance element mounted on the same probe and forming the opposite branch of the bridge. The compensator consisted of tungsten wire 12 in. long and 0.00031 in. in diameter. Before each experimental run the hot-wire was calibrated with a rotating arm calibration arrangement.

The horizontal and vertical fluctuations of the velocity in the boundary layer were measured with a pair of crossed tungsten hot-wire anemometers of the constant-temperature type (5). The length of these wires was 0.1 in. and the diameter 0.00031 in. The response of both the wires and the associated electronic circuit was about 5,000 cps. The compensation for air temperature variation in the boundary layer was accomplished by mounting on the same probe two 2 in. long, 0.00031 in. diameter tungsten wires which comprised the branches of the Wheatstone bridges opposite to those of the hot-wire anemometers.

The tungsten hot-wire anemometers were calibrated in the test section of the wind tunnel and against the mean velocity hot-wire anemometer.

Shear Stress Measurements

The distribution of the Reynolds' stress $\overline{uv}$ was computed from the equations describing the operation of the tungsten crossed hot-wire anemometers. The wall shearing stress was found by extrapolation of the Reynolds' stress profile near the boundary.

Temperature Measurements

The measurement of the mean temperature profiles in the thermal boundary layer, the temperature of the ambient air, and that of the heated boundary were made with copper-constantan thermocouples 0.010 in.

in diameter and mounted on a movable prong. A standard Honeywell recording type potentiometer was used for recording the mean temperatures.

Because of the small size of the thermocouples and the large temperature fluctuations in the thermal boundary layer, an integrator was used for the correct measurement of the mean value of the temperature.

Heat Input Measurements

The electrical power input to each heater strip was measured with an ammeter and voltmeter. The total power input to the boundary was the sum of the input to the 23 electrically isolated heater strips.

Collection of Data

For every run, after the selection of the values of the ambient mean velocity and temperature difference between the ambient air and the surface of the heated boundary, the power input to each strip was adjusted until a surface of uniform temperature was obtained. Following this, data on the pertinent variables were collected along the centerline and at 0.29, 0.96, 3.29, and 9.30 ft from the leading edge of the heated boundary.

The presence of the mass of the 1/2-in. aluminum plate, supporting the heater strips, required a stabilization period of several hours before equilibrium conditions for the temperature were reached. After this period the electrical input was adjusted so that a uniform surface temperature was obtained and data were collected at the abovementioned four stations.

III. DISCUSSION OF RESULTS

The results of this experimental investigation concerning the mean velocity and mean temperature profiles, the local drag coefficient and the distribution of shear, the eddy diffusivity, and the relation between momentum and heat transfer from a smooth, plane boundary with zero pressure gradient are presented in the following pages along with a discussion of the methods used in the analysis of the data.

The Mean Velocity Profile

For neutral stability conditions, when both the plane boundary and the air flowing over it are at the same temperature, the measured velocities in the region of the boundary layer close to the uniform flow were higher than those predicted by the logarithmic law:

$$\frac{U}{U_\star} = \frac{1}{k} \ln \eta + C . \tag{1}$$

This consistent deviation has been observed by several investigators and it extends over a wide range of the Reynolds number. In Fig. 5 a typical mean velocity profile is shown both as actually measured and as predicted by the logarithmic law.

The relatively small variation of this deviation over a wide range of the Reynolds number suggests the possibility that it is a function of the dimensionless distance z/δ from the boundary. Based on this assumption and following Reichardt's (12) modification of the logarithmic law for the same region of flow in closed conduits, an empirical expression was found and added to the logarithmic law modifying it in such a way that both the measured and theoretically predicted values of the mean velocity coinside.

The function best suited for this modification is of the form:

$$\frac{1}{k} \ln \left[\frac{a\,(b - z/\delta\,)}{1 + c\,(1 - z/\delta\,)^{\alpha}} \right] .$$

By proper selection of the constants a , b , c , and α , this function can be made to be equal to zero at $z/\delta = 0$ and have the desired rate of change of slope for increasing values of z/δ . After several trials the following constants were found to fit closely the experimental results: $a = 3$, $b = 2$, $c = 5$, and $\alpha = 1.5$. Thus, the modifying term becomes

$$\frac{1}{k} \ln \left[\frac{3\,(2 - z/\delta\,)}{1 + 5\,(1 - z/\delta\,)^{1.5}} \right]$$

Adding this term to the right side of Eq 1,

$$\frac{U}{U_*} = \frac{1}{k} \ln \eta + \frac{1}{k} \ln \left[\frac{3\,(2 - z/\delta\,)}{1 + 5\,(1 - z/\delta\,)^{1.5}} \right] + C \quad ; \tag{2}$$

or by denoting

$$\frac{U_i}{U_*} = \frac{1}{k} \ln \left[\frac{3\,(2 - z/\delta\,)}{1 + 5\,(1 - z/\delta\,)^{1.5}} \right]$$

and substituting in Eq 2,

$$\frac{U - U_i}{U_*} = \frac{1}{k} \ln \eta + C \quad . \tag{3}$$

The ratio $\frac{U_i}{U_*}$ can be considered as the magnitude of the velocity by which the logarithmic law fails to describe the actual velocity in the boundary layer. The form of this correction term is shown in Fig. 6 as a function of z/δ , and it can easily be observed that it becomes appreciable for values of z/δ larger than 0.2.

In Fig. 5 a typical mean velocity profile is compared to both the logarithmic law and the modified expression of it in the form of Eq 3.

Another approach, seemingly analytical, could be used leading to the same modification. Using the expression

$$\frac{dU}{dz} = \frac{\tau/\rho}{\epsilon} \quad , \tag{4}$$

where both τ and ϵ are functions of z, empirical equations describing the distribution of both τ and ϵ in the boundary layer could be found, which after substitution in Eq 4 would make its integration possible. However, such an approach would be less accurate than the one adopted in this report because of the larger experimental error involved in the measurement of τ and the computation of ϵ than that in the measurement of the mean velocity profile.

A general plot of the mean velocity distribution, compared to both the logarithmic law and Eq 3 for the entire range of Reynolds number used is shown in Fig. 7. For each Reynolds number the value of the Karman constant, k, was computed from the actual mean velocity profile and the wall shearing stress in the following way. The straight line section of the mean velocity profile, plotted on semi-logarithmic paper, was extended to values of $z = 0.1$ in. and $z = 1.0$ in. Then, the respective values of $U_{0.1}$ and $U_{1.0}$ were used in the logarithmic law equation for the analytical determination of k. The variation of the values of k extended from 0.31 to 0.50 without indications of possible correlation with the value of the Reynolds number. An average value of k of about 0.44 seems to fit the experimental data far better than the often used value of 0.40.

The Karman constant k has been the subject of extensive discussions among various investigators. Some feel that it is not a constant at all and refer to it as the Karman number, others that it is a function of Reynolds number. A definite answer to this question will have to await experimental investigations with more accurate data than presently available.

In the case of flow with various lapse rates, that is, with flow of air over a boundary at a higher temperature than that of the ambient air, the effect on the mean velocity profile, as indicated by Richardson number, was limited to a region near the boundary approximately 1/3 of the boundary layer thickness. A typical profile under neutral stability and at a Richardson number of -0.012 is shown in Fig. 8. Unfortunately the experimental equipment limited the Richardson number to values lower than those encountered most frequently in the lower atmosphere, which are approximately -0.12. The primary limiting condition is that of the thickness of the boundary layer: 4.0 in. was about the maximum obtainable.

Figures 9, 10, and 11 show several mean velocity profiles at various Reynolds numbers and for both neutral stability and various lapse rates.

In Fig. 12 several profiles are plotted according to the modified logarithmic law and compared with that at $Ri = 0$. The higher values of wall shear under lapse rates affect the value of the Karman constant k, which increases with decreasing Richardson numbers. This is manifested by the steeper profiles and higher constants as it can be observed in the figure.

The Mean Temperature Profile

The points of inception for both the momentum and thermal boundary layers are shown in the definition sketch of Fig. 4. The growth of the thermal boundary layer was found to be a function of both the ambient velocity of the air and the magnitude of the temperature difference between the heated boundary and the ambient air. The thickness of the thermal boundary layer invariably increased fast enough to be either equal to the momentum boundary layer thickness near the end of the heated boundary for an ambient velocity of 35 fps, or thicker than that for lower velocities.

Figures 9, 10, and 11 show the profiles at 0.96, 3.29, and 9.30 ft from the leading edge of the heated boundary, along the centerline, and for ambient velocities of 10, 17, and 35 fps. Comparing the corresponding mean velocity and mean temperature profiles in these figures, one can see clearly that the history of the development of both boundary layers is the same. At the end of the boundary the two profiles are similar in shape and for longer lengths of heated boundary they will probably be identical. This comparison can be carried out better by use of Fig. 13, where corresponding mean velocity and mean temperature profiles are plotted for the same dimensionless distances from the boundary, the 45° straight line representing the case of identical profiles. From this figure it can be observed that the lack of similarity of the two profiles is a function of the Richardson number.

The Local Drag Coefficient and the Distribution of Shear

The local drag coefficient was determined from the shear distribution profile by extrapolating it near the boundary. The cross-wire anemometer, used in the determination of the shear profile, measures only the Reynolds shear, $\overline{uv}$, and owing to its physical size it could not be located nearer than about 1/8-in. from the boundary. However, at this distance the viscosity effects are of the order of a few per cent of the total shear. Therefore, the Reynolds shear is approximately the total shear at the points where the measurements were taken.

For neutral stability conditions Fig. 14 shows the experimental results as well as those predicted by the 1/7-power law and Schultz-Grunow's equation. The latter fits the experimental points better. This figure can also be considered as a verification of the accuracy of the instrument used for the measurement of shear.

In the case of flow with various lapse rates, the local drag coefficient is a function of both Reynolds and Richardson numbers. By definition Richardson number is the ratio of the bouyancy forces to those of inertia:

$$Ri = \frac{g}{(T_a)_{abs}} \frac{\frac{dT}{dz}}{\left(\frac{dU}{dz}\right)^2} \quad . \tag{5}$$

However, Eq 5 depends on the distance z from the boundary as well as the distance x along it. To overcome this limitation in this investigation, the Richardson number was formed as follows:

$$Ri_\delta = \frac{g}{(T_a)_{abs}} \frac{\frac{\Delta T}{\delta_t}}{\left(\frac{U_o}{\delta}\right)^2} \quad . \tag{6}$$

Thus, a single number could be used to characterize the entire profile. This modification, however, is valid only in the case that both the mean velocity and mean temperature profiles are approximately the same.

Another dimensionless parameter very close in form to the Richardson number was formed in the following way:

$$Ri_x = \frac{g \ \Delta T \ x}{(T_a)_{abs} \ U_o^2} \quad . \tag{7}$$

This parameter, since it is a function of the distance along the heated boundary, was used to correlate the local drag coefficient and Reynolds number.

Figure 15 shows the relation between the local drag coefficient and the modified Richardson number as given by Eq 6. It has been observed that such a relation is true only in the case that the two boundary layers are of approximately equal thickness. Attempts to include the data taken in the first foot length of the heated boundary, where the thickness of the thermal boundary layer is less than half of that of the momentum, resulted in considerable scatter of the points. In other words, the shape of the two profiles must be approximately the same for such a relation to be consistent. In this form of presentation of the results the effect of the Reynolds number is not apparent.

In Fig. 16 the local drag coefficient is combined with the dimensionless parameter of Eq 7 and plotted as a function of Reynolds number and ambient air velocity. Several attempts of different combinations of the four parameters involved failed to result in one curve for all the experimental points. Instead, an unsystematic scatter of the points indicated the desirability of presenting the data as shown in Fig. 16.

Profiles of the shear distribution in the boundary layer and at various distances along the boundary and for various ambient velocities are shown in Figs. 17, 18 and 19. The vertical and horizontal turbulence intensities are shown in Figs. 20, 21 and 22. For purposes of comparison, the distributions at both neutral stability and various lapse rates are plotted in the same figures.

The Eddy Diffusivity

By analogy to the molecular diffusivity the eddy diffusivity could be defined as

$$\epsilon = -\frac{\overline{uv}}{dU/dz} \quad . \tag{8}$$

Therefore, the determination of the distribution of ϵ in a particular section in the boundary layer could be accomplished by the measurement of the Reynolds stress, $\overline{uv}$, with a crossed hot-wire anemometer and the mean velocity profile. In this study the distribution of $\overline{uv}$ was directly measured and the mean velocity gradient was obtained by the following three different methods:

(a) The velocity distribution was assumed to be logarithmic as given by Eq 1. Differentiating Eq 1

$$\frac{dU}{dz} = \frac{U_*}{kz} \quad ,$$

and substituting in Eq 8

$$\epsilon = -\frac{\overline{uv}}{U_*/kz} \quad ,$$

or

$$\epsilon = -\frac{kz\overline{uv}}{U_*} \quad .$$

Substituting

$$U_* = \sqrt{-\overline{uv}}$$

and dividing by $U_o\delta$, to obtain a dimensionless expression, the final form of the eddy diffusivity distribution becomes

$$\frac{\epsilon}{U_o\delta} = -\frac{kz\sqrt{-\overline{uv}}}{U_o\delta} \quad . \tag{9}$$

(b) The velocity distribution was assumed to conform with the modified expression as given by Eq 2. Consequently,

$$\frac{dU}{dz} = \frac{\sqrt{\overline{uv}}}{\delta\, k}\left[\frac{1}{z/\delta} - \frac{1}{2 - z/\delta} + \frac{7.5\,(1 - z/\delta)^{1/2}}{1 + 5\,(1 - z/\delta)^{1.5}}\right].$$

Substituting this expression in Eq 8 and dividing by $U_o\delta$

$$\frac{\epsilon}{U_o\delta} = -\frac{k\sqrt{\overline{uv}}}{U_o\left[\frac{1}{z/\delta} - \frac{1}{(2 - z/\delta)} + \frac{7.5\,(1 - z/\delta)^{1/2}}{1 + 5\,(1 - z/\delta)^{1.5}}\right]} . \quad (10)$$

(c) The velocity gradient $\frac{dU}{dz}$ was obtained from numerical differentiation of the mean velocity profile, as actually measured, and substituted in Eq 8.

For neutral stability conditions the results of these three different methods of obtaining the eddy diffusivity profile are shown in Fig. 23 in a dimensionless form. A comparison of the three plots indicates that the assumption of a logarithmic distribution gives results that are twice as large as the direct method of numerical differentiation. Also, the maximum value of ϵ is at about $z/\delta = 0.70$ instead of 0.45. However, the results obtained from Eq 10, which is based on the modified logarithmic laws as given by Eq 2, are approximately the same as those obtained by numerical differentiation.

This comparison, therefore, indicates conclusively that the modified logarithmic law represents the actual distribution of the mean velocity in the boundary layer and a more accurate analytical expression for the determination of the distribution of ϵ. The numerical differentiation of the measured velocity profile, although more direct, is susceptible to experimental errors that result in an excessive scatter of the points as indicated in Fig. 23 (c).

For values of $z/\delta > 1$, the distribution of ϵ has been extrapolated to indicate its magnitude in the ambient air flow. This magnitude is a function of the ambient air turbulence level and cannot be determined with the instrumentation employed because both the Reynolds stress and the velocity gradient approach the value of zero simultaneously.

In Fig. 24 the eddy diffusivity, as determined by Eq 10, is shown for neutral stability and various lapse rates. The use of either Ri_δ or Ri_x to indicate the magnitude of the lapse rate failed to show a systematic trend. For the highest lapse rate, the maximum value of ϵ is about seven times that for neutral stability.

<u>The Relation Between Momentum and Heat Transfer</u>

In 1939 Karman, using Reynolds analogy between heat and momentum transfer, derived the following equation, which relates the local drag coefficient to that of heat transfer:

$$\frac{1}{C_H} = \frac{2}{C_f} + 5\left(\frac{2}{C_f}\right)^{1/2}\left\{\sigma - 1 + \ln\left[1 + \frac{5}{6}(\sigma - 1)\right]\right\} . \qquad (11)$$

Equation 11 was modified by Cermak for evaporation by substituting $C_e = \frac{E}{\rho g U_o \Delta C}$ for C_H. Assuming a 1/7-power relation for the velocity distribution, Cermak obtained the following equation for the range of $10^3 \leq R_\star \leq 10^5$:

$$N^{-1} = \frac{6.23\ R_\star^{-8/9}}{(x'/x)^{4/45}} - \frac{3.77\ R_\star^{-1}}{(x'/x)^{1/10}} , \qquad (12)$$

where $N = \frac{Ex}{\Delta C\ \nu_e}$ and $R_\star = \frac{U_\star x}{\nu_e}$.

Substituting Nu and Pe for N and $R_\star$ respectively in Eq 12,

$$Nu^{-1} = \frac{6.23\ Pe^{8/9}}{(x'/x)^{4/45}} - \frac{3.77\ Pe^{-1}}{(x'/x)^{1/10}} . \qquad (13)$$

This equation relates the heat and the momentum transfer, and it is based on the Reynolds analogy. The Nusselt number indicates the heat input and the Peclet number describes the momentum transfer $(Pe = \frac{U_* x}{K_t})$.

Further, Eq 13 can be modified by substituting:

$Nu = (St)(Pe)$,

and thus becomes:

$$St^{-1} = \frac{6.23\ Pe^{1/9}}{(x'/x)^{4/45}} - \frac{3.77}{(x'/x)^{1/10}} \ . \qquad (14)$$

In Fig. 25, the data obtained in this experimental investigation are compared to Eq 13 and in Fig. 26 to Eq 14. On the same figures, Sutton's theory is also compared to the data. According to this theory the evaporation from a plane surface can be expressed by the following equation:

$$\frac{E}{\nu \Delta C} = F_1(n,\ k) \left(\frac{U_* x}{\nu}\right)^{2(2+n)} , \qquad (15)$$

where

$$F_1(n,k) = (2+n)^{\frac{4}{2+n}} \ \frac{1}{2\pi} \sin\frac{2\pi}{2+n} \Gamma\left(\frac{2}{2+n}\right)\left(\frac{\pi k^2}{2}\right)^{\frac{1-n}{2+n}} n^{\frac{-n}{2+n}} (1-n)^{\frac{-1}{2+n}} (2n-2)^{\frac{-2(1-n)}{2+n}} \ .$$

Substituting Nu for $\frac{E}{\nu \Delta C}$ and Pe for $\frac{U_* x}{\nu}$ in the above equation,

$$Nu = F_1(n,\ k)\ Pe^{\frac{2}{2+n}} \qquad (16)$$

or

$$St = F_1(n,\ k)\ Pe^{\left(\frac{2}{2+n} - 1\right)} , \qquad (17)$$

which relates the momentum and the heat transfer.

A comparison of Eqs 13, 14, 16, and 17 with the data obtained indicates that Sutton's theory does not agree as closely to the data as Eqs 13 and 14 which are based on Reynolds analogy, for the lower range of Peclet number.

Miscellaneous Remarks

The thicknesses of the momentum and the thermal boundary layers defined by δ and δ_t respectively, are mean values of quantities having a considerable range of fluctuations. This intermittancy of the thickness of the boundary layers should be expected since actually the boundary layer is a transition region in which the turbulence intensities vary from zero in the immediate vicinity of the boundary to a maximum at about half the distance to the uniform flow and then to a lower level, which is the turbulence level of the ambient air. If one considers the foregoing and the random nature of turbulence, then it could be concluded that random fluctuations of lower frequencies will be expected to reach the uniform flow.

In this investigation, as well as in all cases where the variables involved are fluctuating quantities, the collection of data is a sampling process and the accuracy of the results depends on the accuracy of the instrumentation employed and the representativeness of the samples. The latter can be improved considerably by the use of integrators attached to all instruments, including those that have large time constants. Thus the human error involved in reading the fluctuating needle of an indicating meter will be eliminated.

IV. SUMMARY OF RESULTS

Within the experimental range, the results of this study can be summarized in the following way:

(1) The mean velocity distribution in the boundary layer for both neutral stability and various lapse rates is described more accurately by the "modified logarithmic law'

$$\frac{U - U_i}{U_*} = \frac{1}{k} \ln \eta + C$$

than by the logarithmic law.

Under various lapse rates the mean velocity distribution, plotted as a function of $\frac{U}{U_o}$, is not affected appreciably by the Richardson number because of the small negative numbers obtainable with the experimental equipment used.

For neutral stability, the average value of the Karman constant k is about 0.44. For various lapse rates, this value increases considerably because of the increase of the wall shearing stress.

(2) The distribution of the mean temperature in the thermal boundary layer becomes similar to that of the mean velocity at the sections of the heated boundary where the thickness of the momentum and thermal boundary layers are of the same magnitude.

(3) The local drag coefficient increases considerably with increasing negative Richardson numbers.

(4) The distribution of the eddy diffusivity in the momentum boundary layer is considerably more accurately computed

by the use of the "modified logarithmic law" than by the use of the logarithmic law. With various lapse rates, Richardson number affects the eddy diffusivity considerably.

(5) For the experimental range covered in this study, Karman's modification of Reynolds analogy between momentum and heat transfer is in better agreement with the experimental results than Sutton's theory.

REFERENCES

1. Cermak, J. E. and Lin, P. N. Vapor transfer by forced convection from a smooth, plane boundary. Department of Civil Engineering, Colorado A and M College, Report No. 55JEC1, January 1955.

2. Corrsin, Stanley. Extended application of the hot-wire anemometer. National Advisory Committee for Aeronautics TN 1864, April 1949.

3. Elias, Franz. The transference of heat from a hot plate to an air stream. National Advisory Committee for Aeronautics TM 614, April 1931.

4. Goldstein, S. Modern developments in fluid dynamics. Oxford at the Clarendon Press, Vol. II, 1950.

5. Hubbard, P. G. Application of a D-C negative-feedback amplifier to compensate for the thermal lag of a hot-wire anemometer. Proceedings of the National Electronics Conference, Vol. 4, 1948.

6. Karman, Th. The analogy between fluid friction and heat transfer. Trans., ASME, Vol. 61, p. 705-10, November 1939.

7. Klebanoff, P. S. and Diehl, Z. W. Some features of artificially thickened fully developed turbulent boundary layers with zero pressure gradient. National Advisory Committee for Aeronautics TN 2475, October 1951.

8. Klebanoff, P. S. Characteristics of turbulence in a boundary layer with zero pressure gradient. National Advisory Committee for Aeronautics TN 3178, July 1954.

9. Lin, C. C. and Shen, S. F. Studies of von Karman's similarity theorem and its extension to compressible flows. A critical examination of similarity theory for incompressible flows. National Advisory Committee for Aeronautics TN 2541, November 1951.

10. Prandtl, L. The essentials of fluid dynamics, London, Blackie and Son, 1953.

11. Reichardt, H. Der einfluss der wandnahen strömung auf den turbulenten warmeübergang. Mitteil No. 3, of Max Planck Inst., Göttingen 1950.

12. Reichardt, H. Vollstandige darstellung der turbulenten geschwindigkeitsverteilung in glätten leitungen. ZAMM, July 1951. p. 208-18.

13. Scardon, M. D. and Warshawsky, Isidore. Experimental determination of time constants and Nusselt number for bare-wire thermocouple in high-velocity air streams and analytic approximation of conduction and radiation errors. National Advisory Committee for Aeronautics TN 2599, January 1952.

14. Schubauer, G. B. and Klebanoff, P. S. Theory and application of hot-wire instruments in the investigation of turbulent boundary layers. National Advisory Committee for Aeronautics Adv. Conf. Report 5K27, March 1946.

15. Schultz-Grunow, F. New frictional resistance law for smooth plates. National Advisory Committee for Aeronautics TM 986, September 1941.

16. Sutton, O. G. Wind structure and evaporation in a turbulent atmosphere. Proc., Royal Society (London), A40, p. 701-22, 1934.

17. Sutton, O. G. Micrometeorology. New York, McGraw-Hill, 1953.

18. Theodorides, P. J. A review of investigations on turbulent flow with heat transfer at smooth walls. U. S. Naval Ordnance Laboratory. Navord Report 2958, White Oak, Maryland, November 4, 1953.

LIST OF FIGURES

Figure	
1	Plan of wind tunnel
2	Test section
3	Heated boundary
4	Definition sketch for momentum and thermal boundary layers
5	Typical mean velocity profile for neutral stability $R_{x'} = 7.75 \times 10^5$
6	Distribution of correction term $k \frac{U_i}{U_*}$
7	Mean velocity distribution for neutral stability $2.9 \times 10^5 < R_{x'} < 2.75 \times 10^6$
8	Typical mean velocity profiles for neutral stability and lapse rates
9	Mean velocity and temperature profiles for $U_o = 10$ fps
10	Mean velocity and temperature profiles for $U_o = 17$ fps
11	Mean velocity and temperature profiles for $U_o = 35$ fps
12	Mean velocity distributions for various lapse rates
13	Relation between mean velocity and mean temperature
14	Variation of local drag coefficient with Reynolds number for neutral stability
15	Local drag coefficient for various lapse rates
16	Variation of drag coefficient with Reynolds number, Richardson number, and ambient velocity
17	Shear profiles for $U_o = 10$ fps
18	Shear profiles for $U_o = 17$ fps
19	Shear profiles for $U_o = 35$ fps
20	Profiles of vertical and horizontal intensities of turbulence for $U_o = 10$ fps

Figure

21 Profiles of vertical and horizontal intensities of turbulence for $U_o = 17$ fps

22 Profiles of vertical and horizontal intensities of turbulence for $U_o = 35$ fps

23 Eddy diffusivity distribution for neutral stability:
(a) assuming logarithmic velocity distribution,
(b) assuming modified logarithmic velocity distribution, and
(c) numerical differentiation of the velocity profile as measured

24 Eddy diffusivity distributions assuming modified logarithmic velocity distribution

25 Variation of Nusselt number with Peclet number

26 Variation of Stanton number with Peclet number

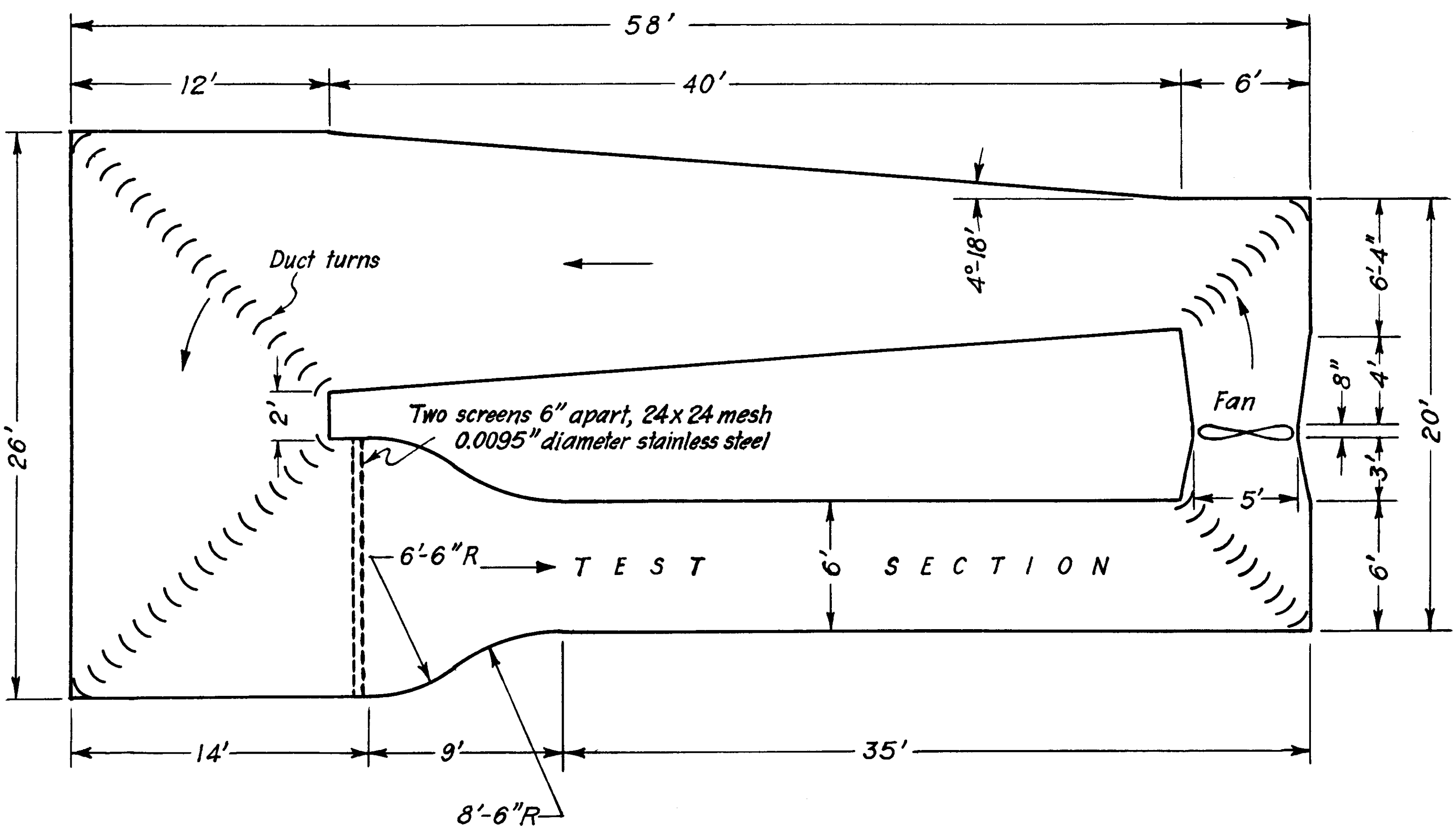

Fig. 1 Plan of wind tunnel

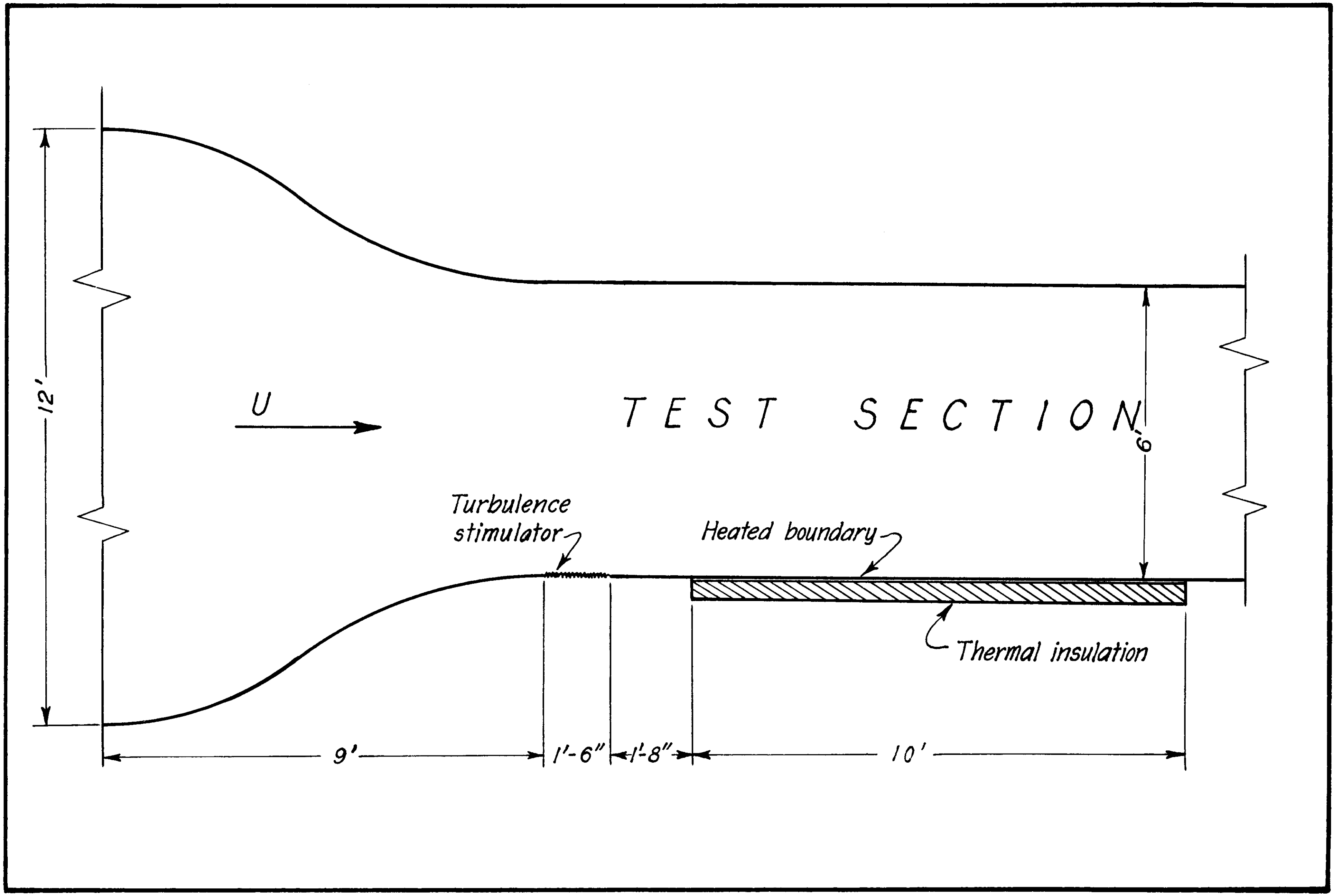

Fig. 2 Test section

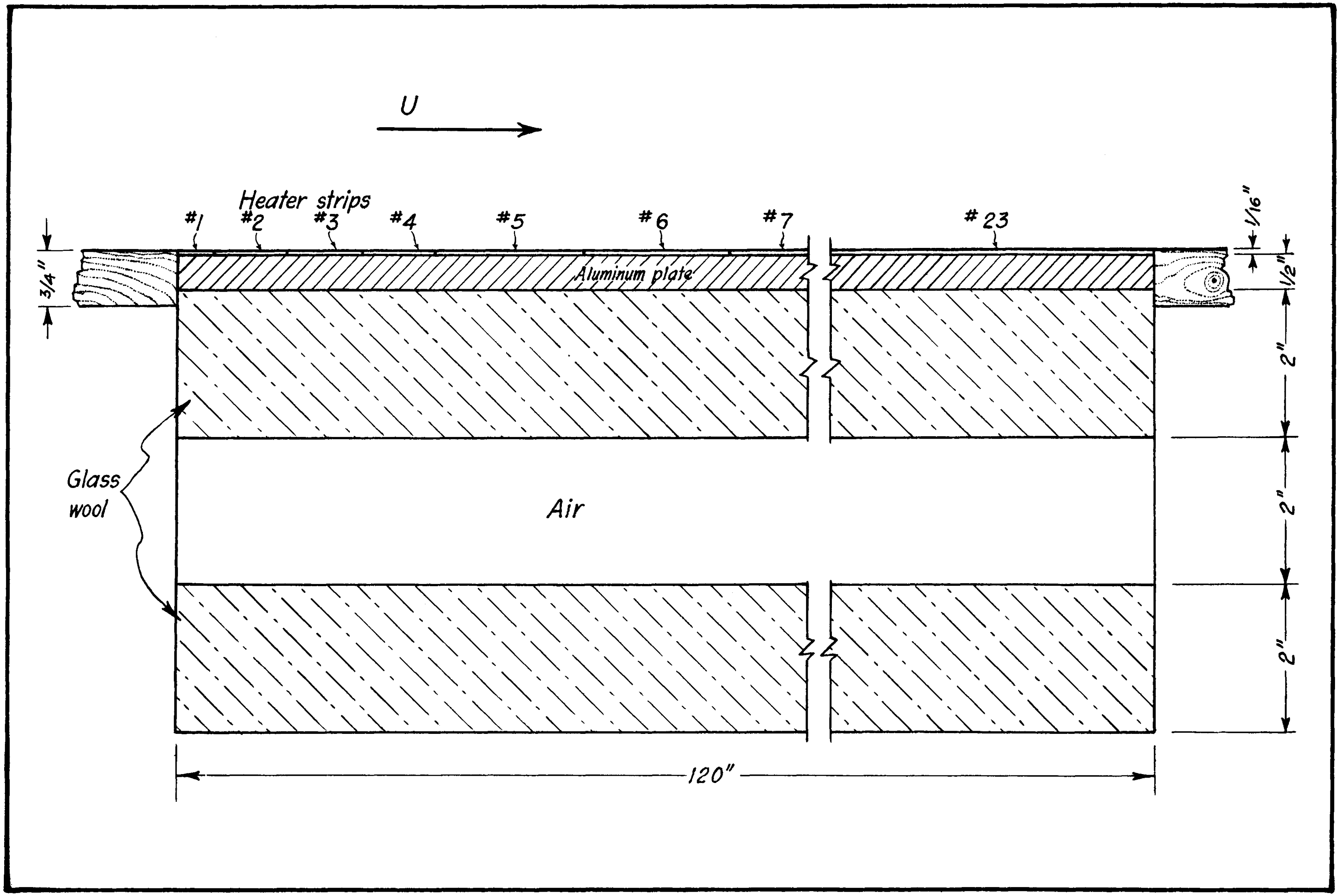

Fig. 3 Heated boundary

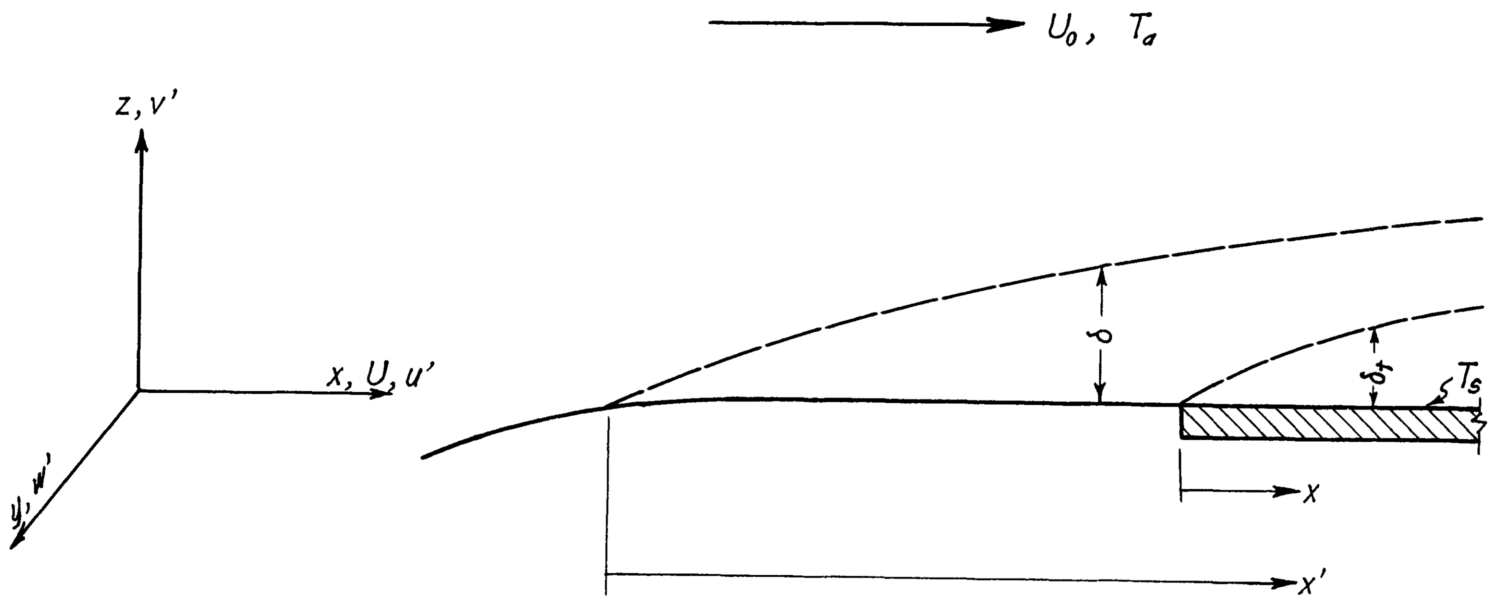

Fig. 4 Definition sketch for momentum and thermal boundary layers

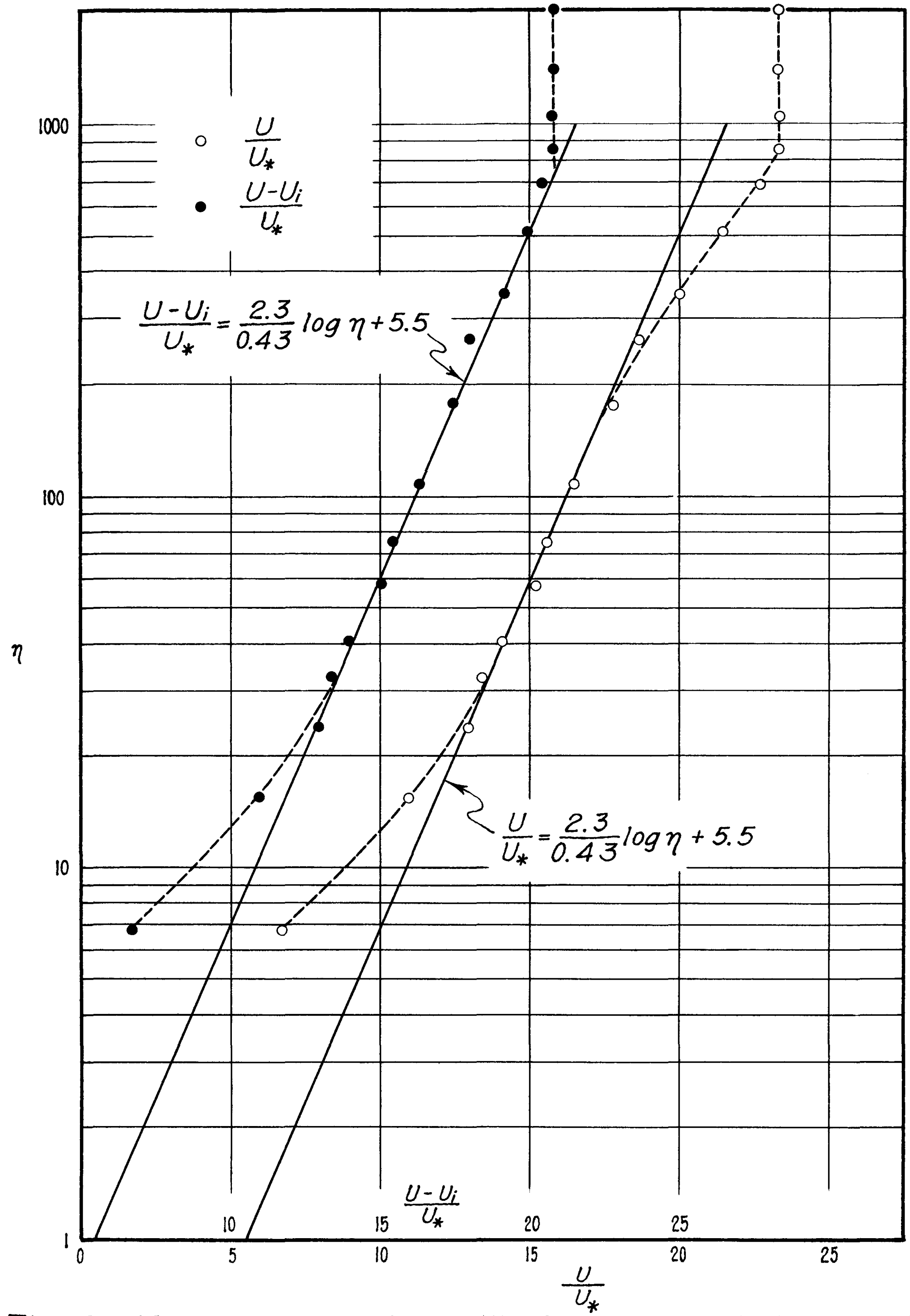

Fig. 5 Typical mean velocity profile for neutral stability $R_{x'}=7.75\times10^5$

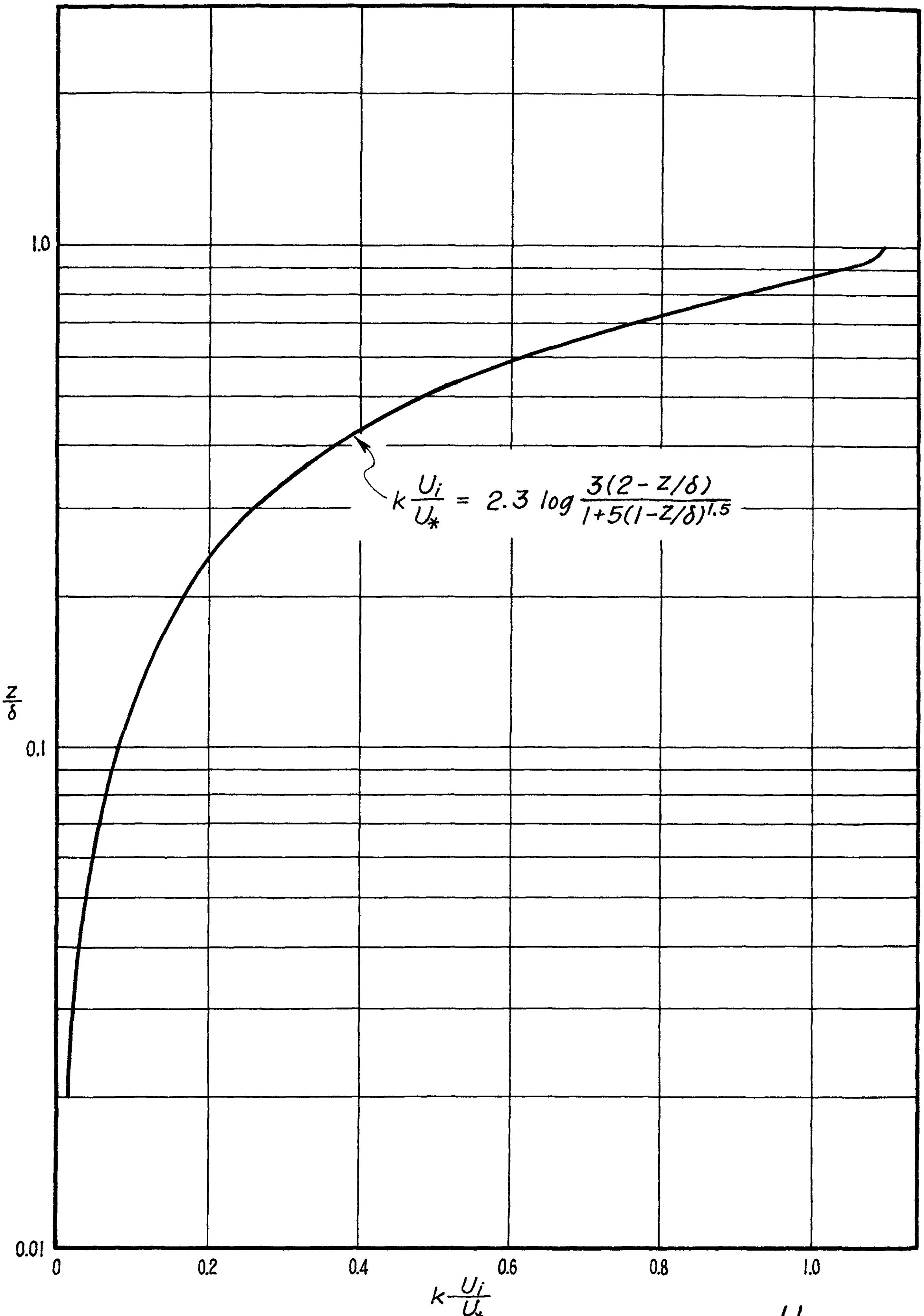

Fig. 6 Distribution of correction term $k\frac{U_i}{U_*}$

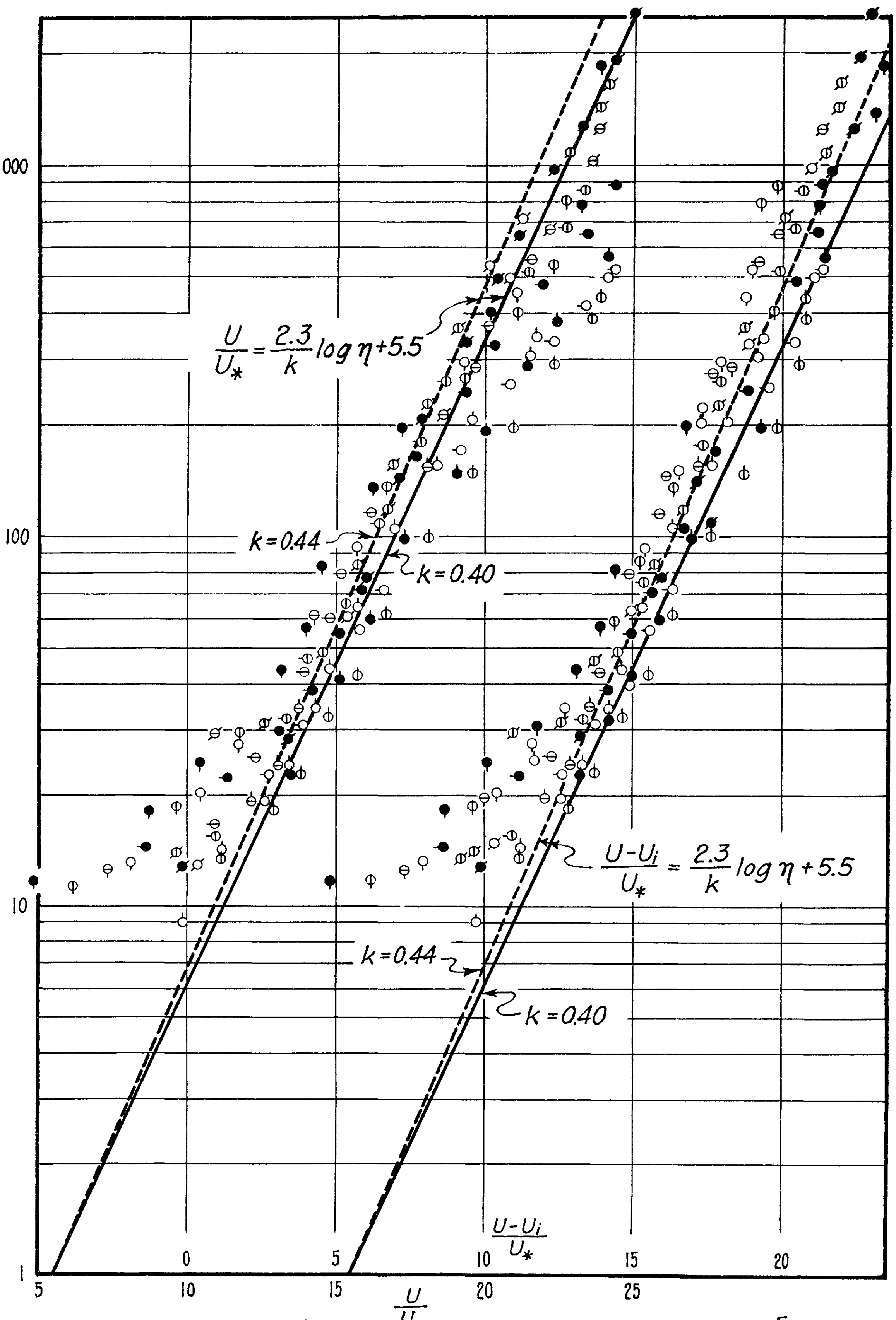

Fig. 7 Mean velocity distribution for neutral stability $2.9\times10^5 < R_{x'} < 2.75\times10^6$

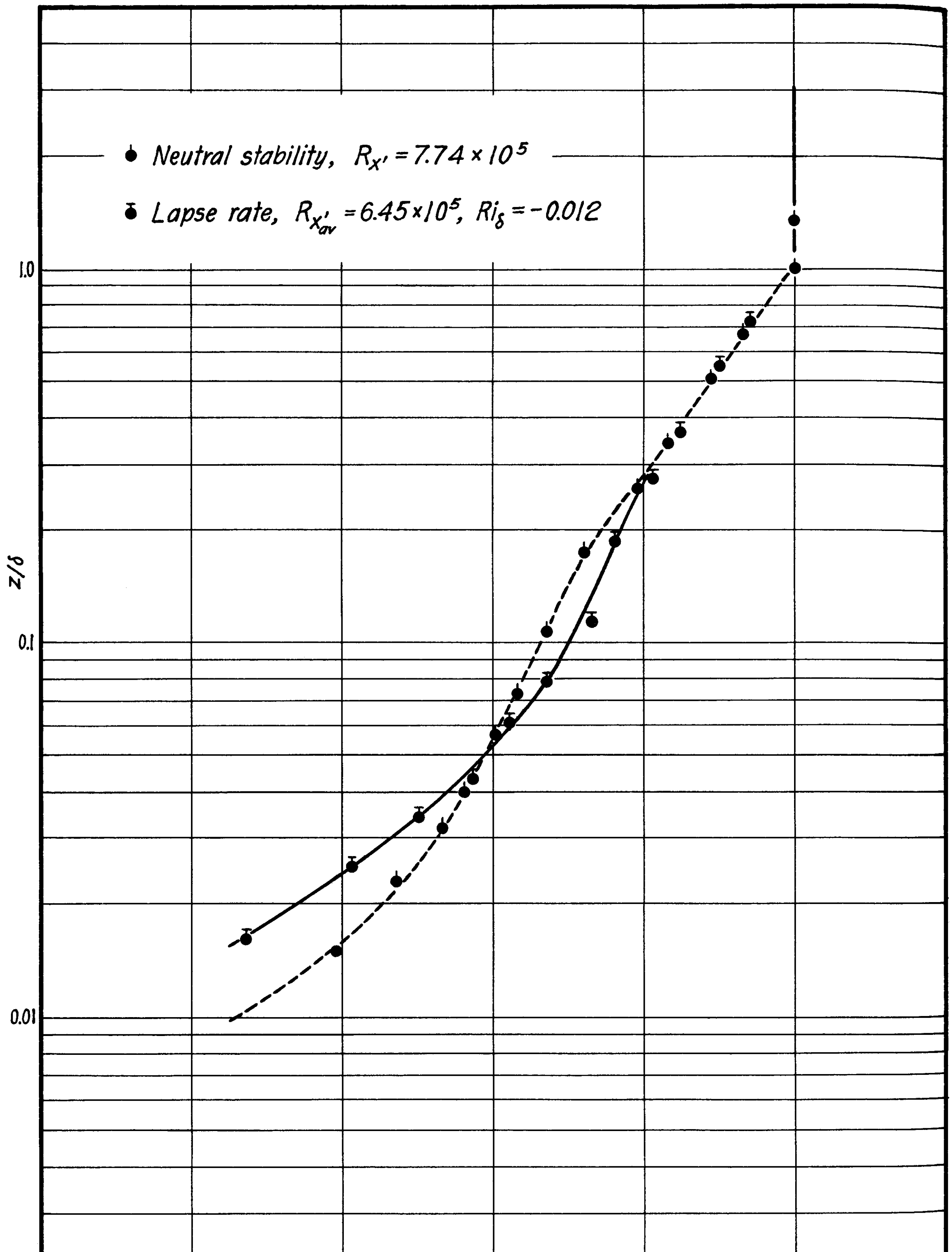

Fig.8 Typical mean velocity profiles for neutral stability and lapse rates

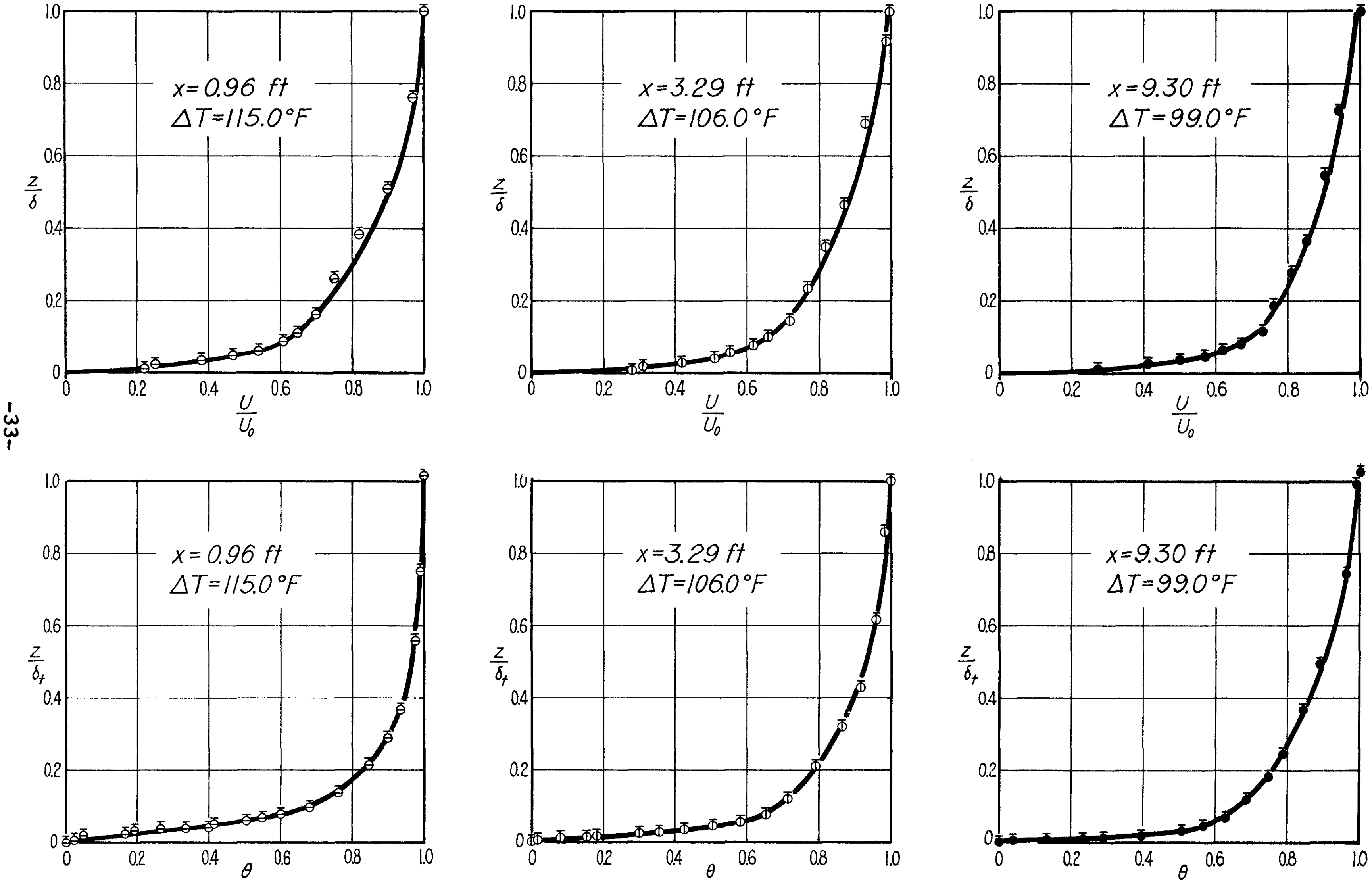

Fig.9 Mean velocity and temperature profiles for U_0 =10 fps

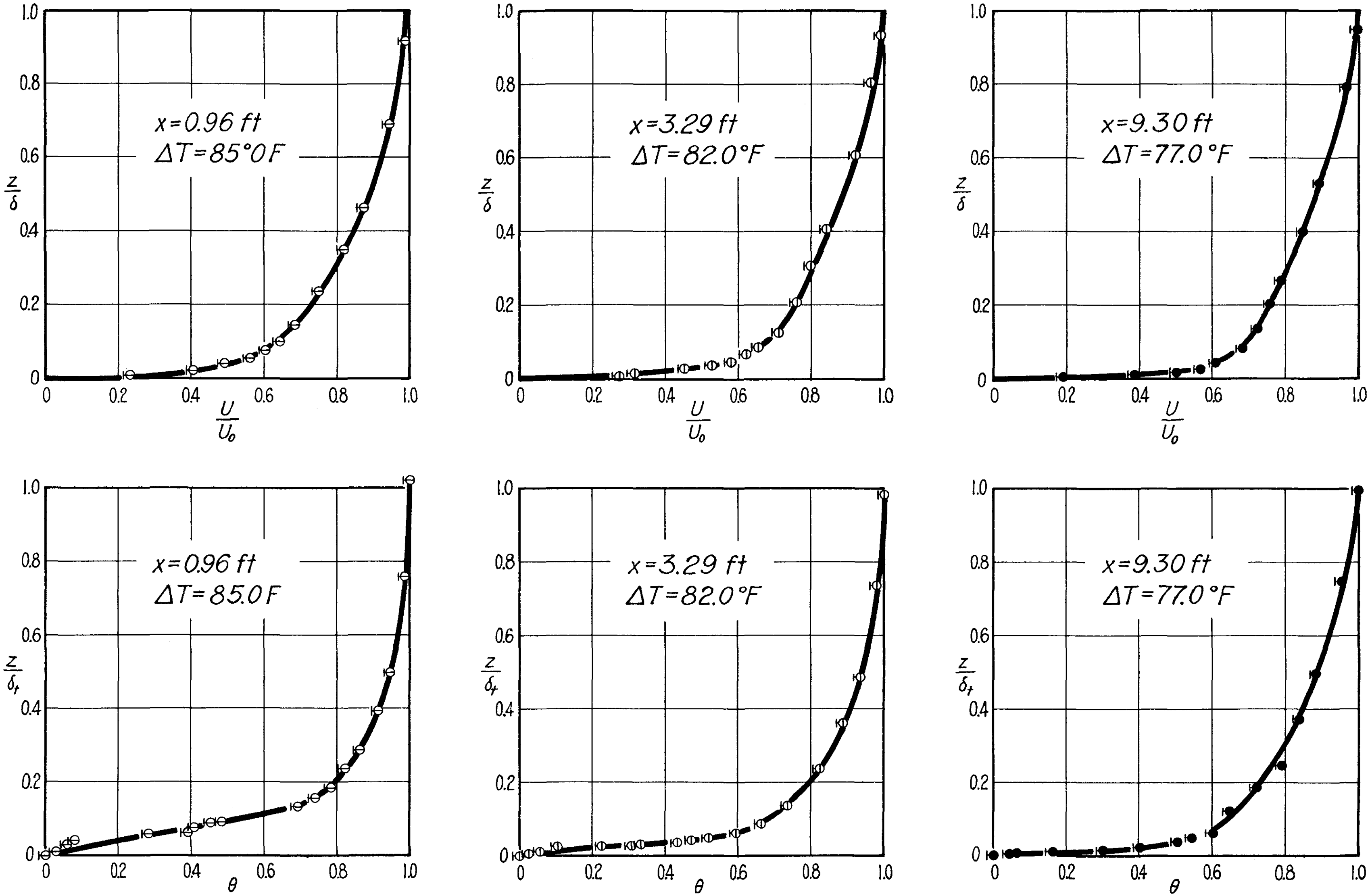

Fig. 10 Mean velocity and temperature profiles for $U_0 = 17$ fps

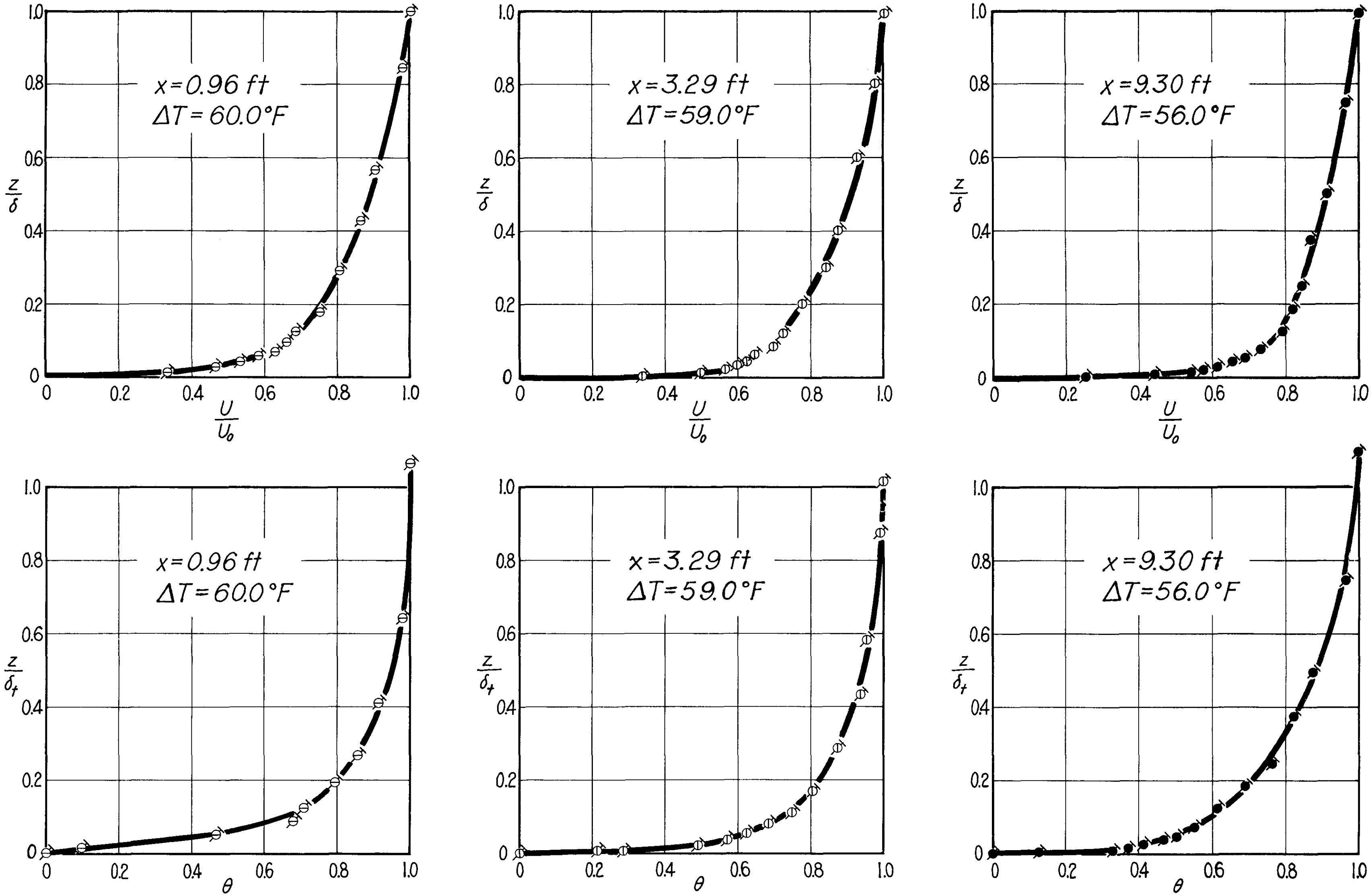

Fig. 11 Mean velocity and temperature profiles for U_0 = 35 fps

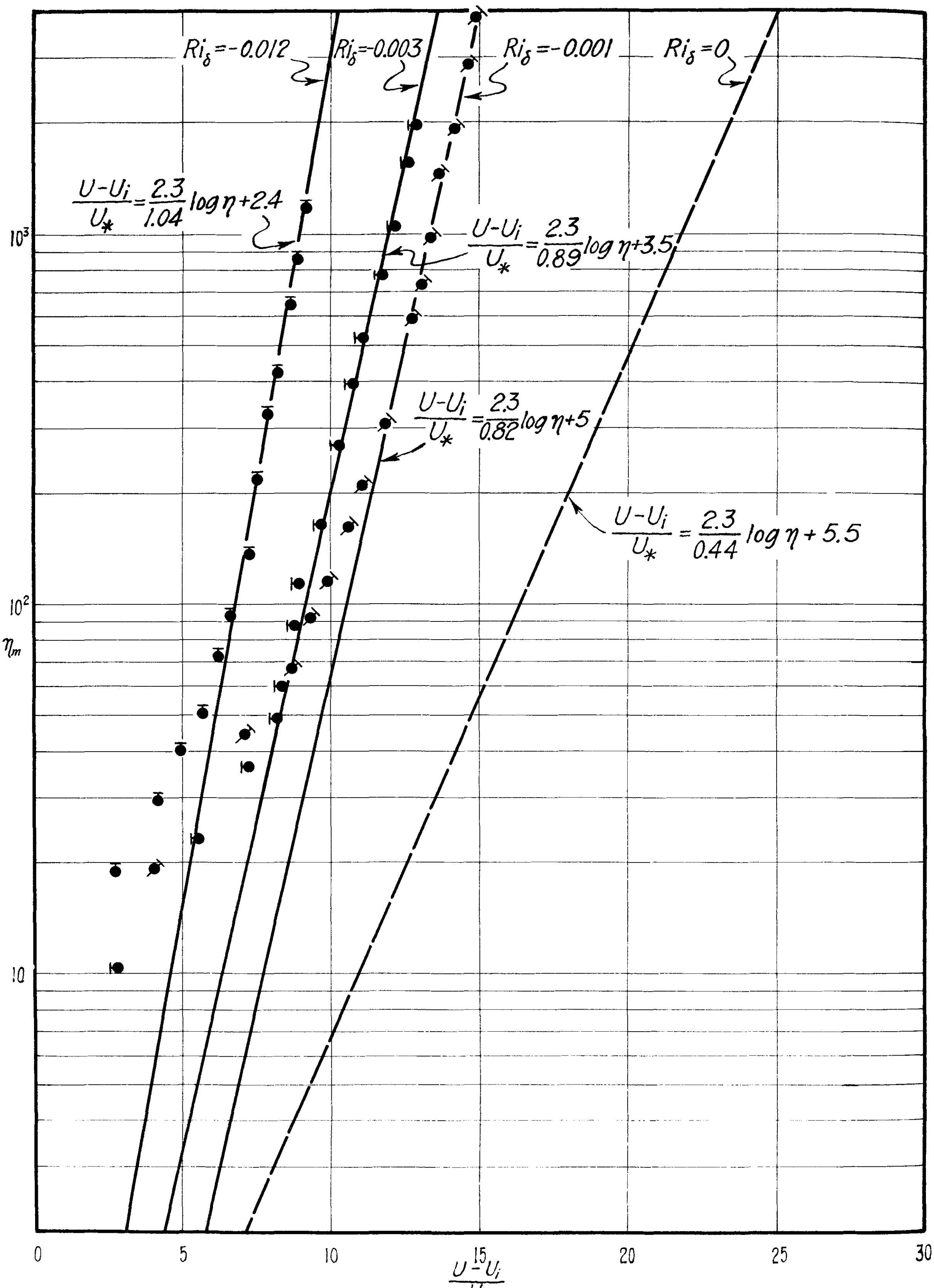

Fig.12 Mean velocity distributions for various lapse rates

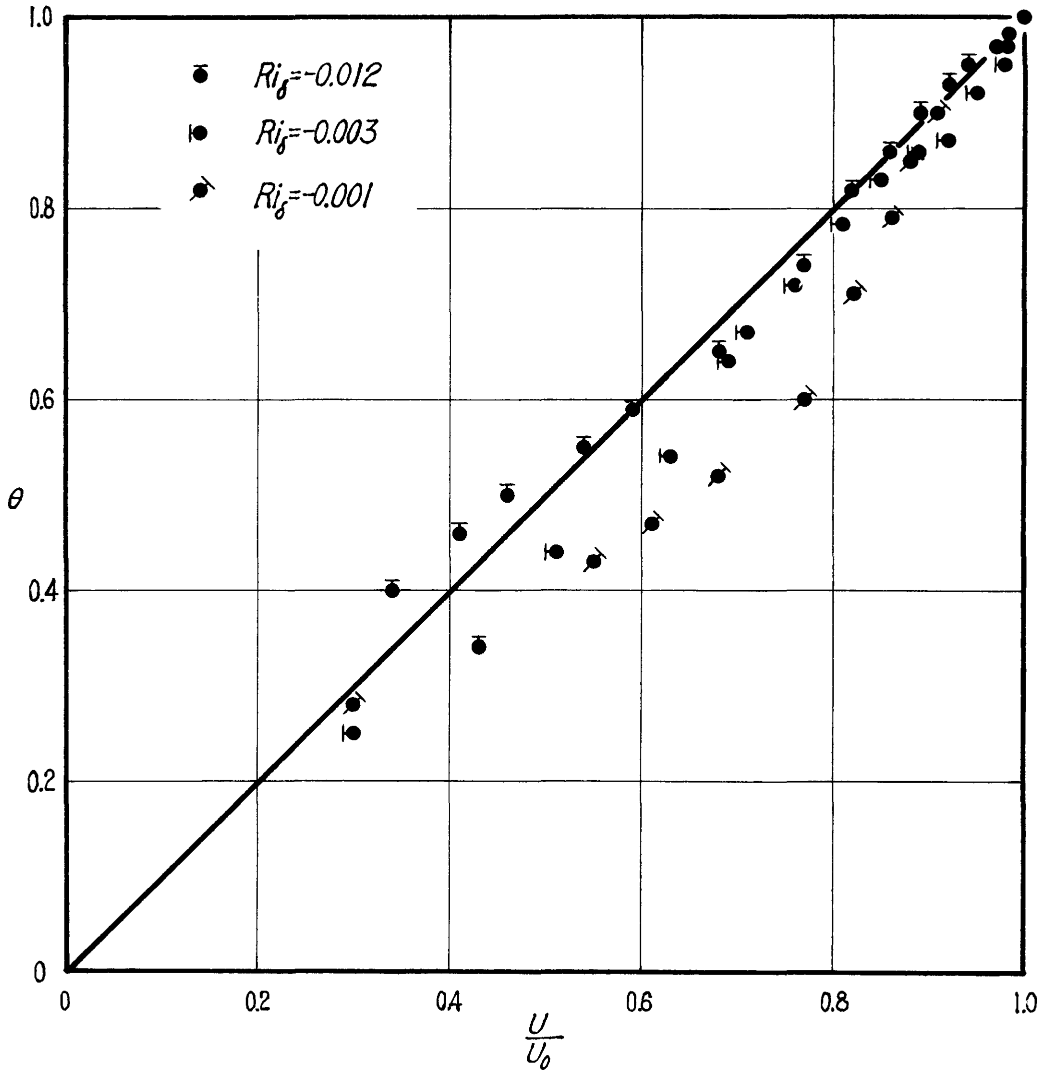

Fig. 13 Relation between mean velocity and mean temperature

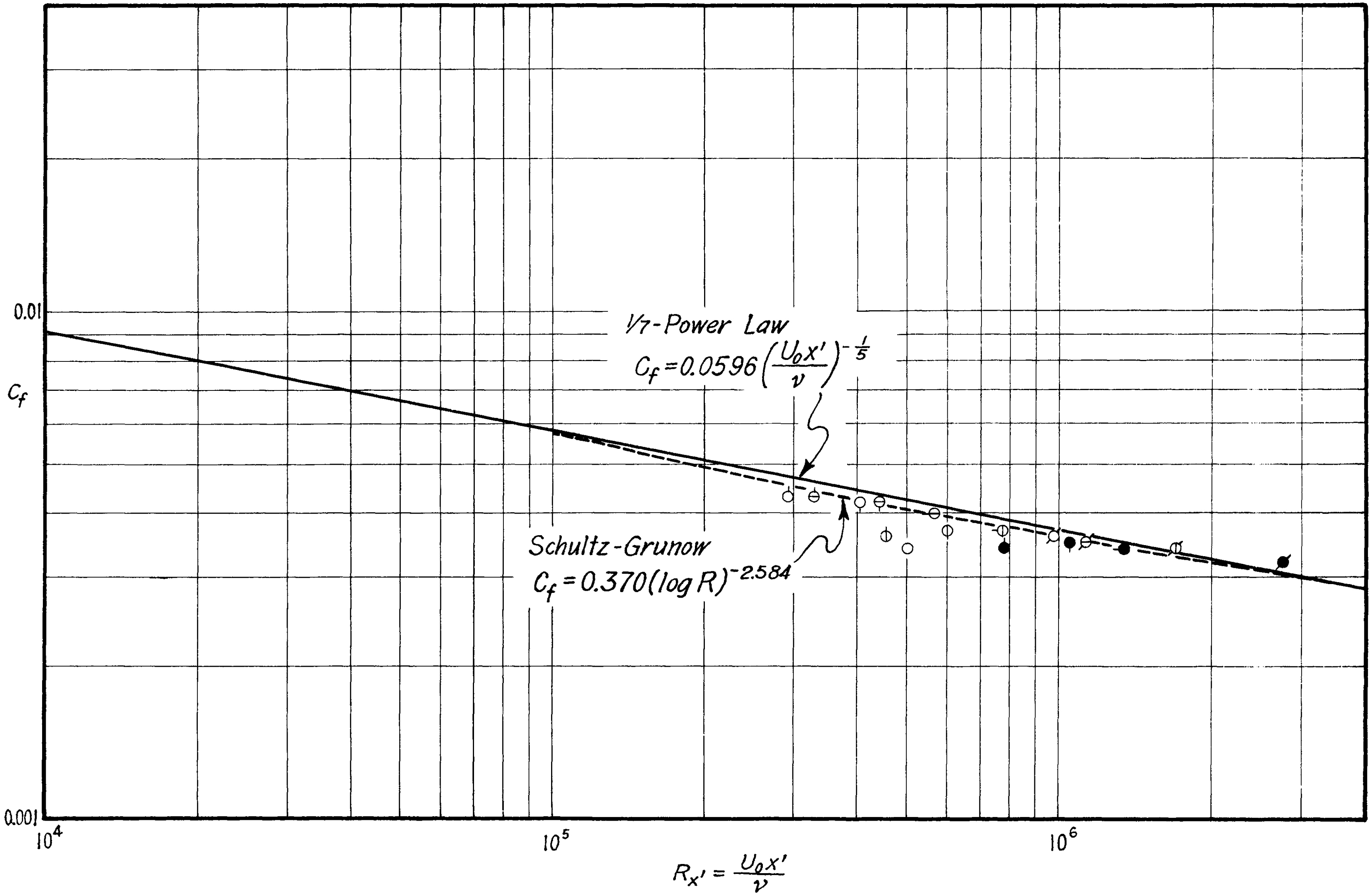

Fig. 14 Variation of local drag coefficient with Reynolds number for neutral stability

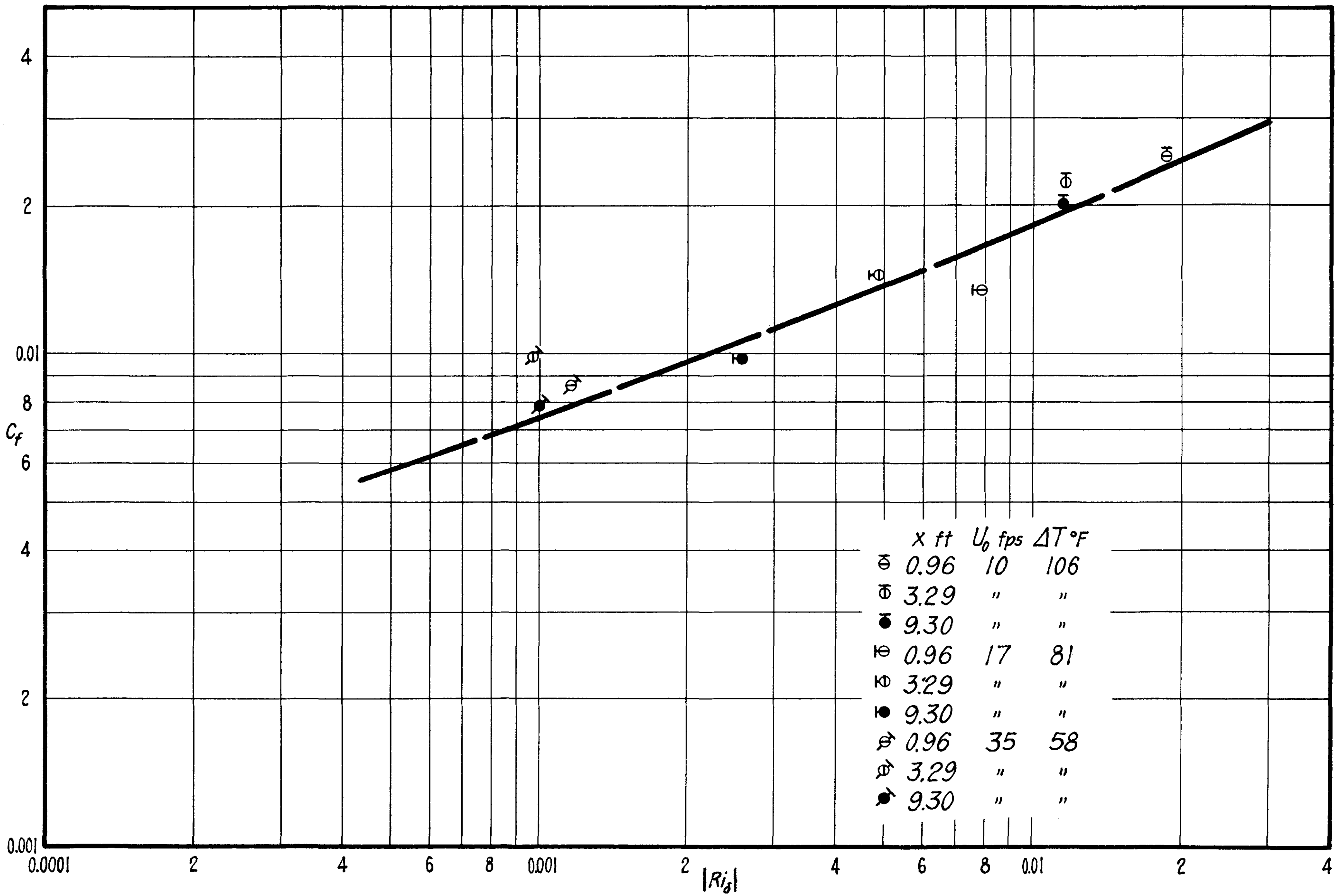

Fig. 15 Local drag coefficient for various lapse rates

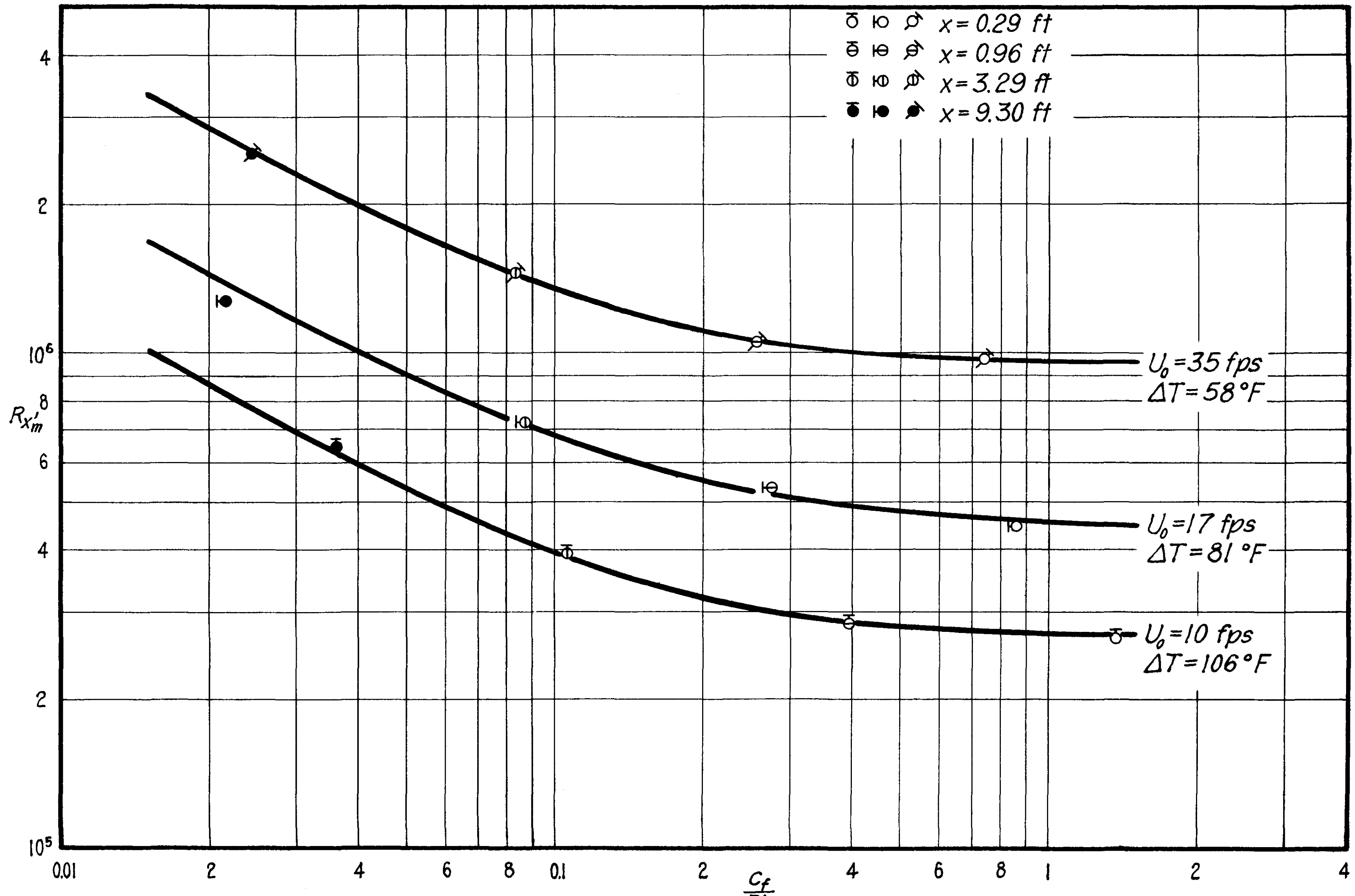

Fig. 16 Variation of drag coefficient with Reynolds number, Richardson number, and ambient velocity

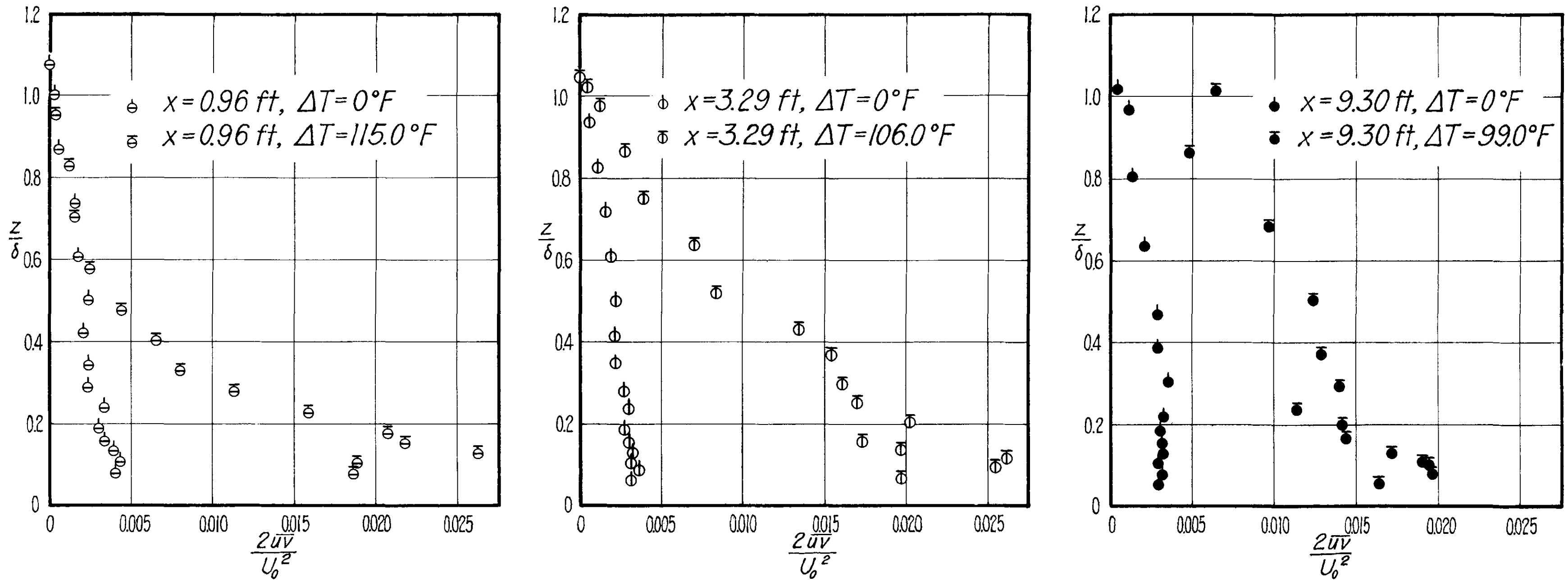

Fig. 17 Shear profiles for $U_0 = 10$ fps

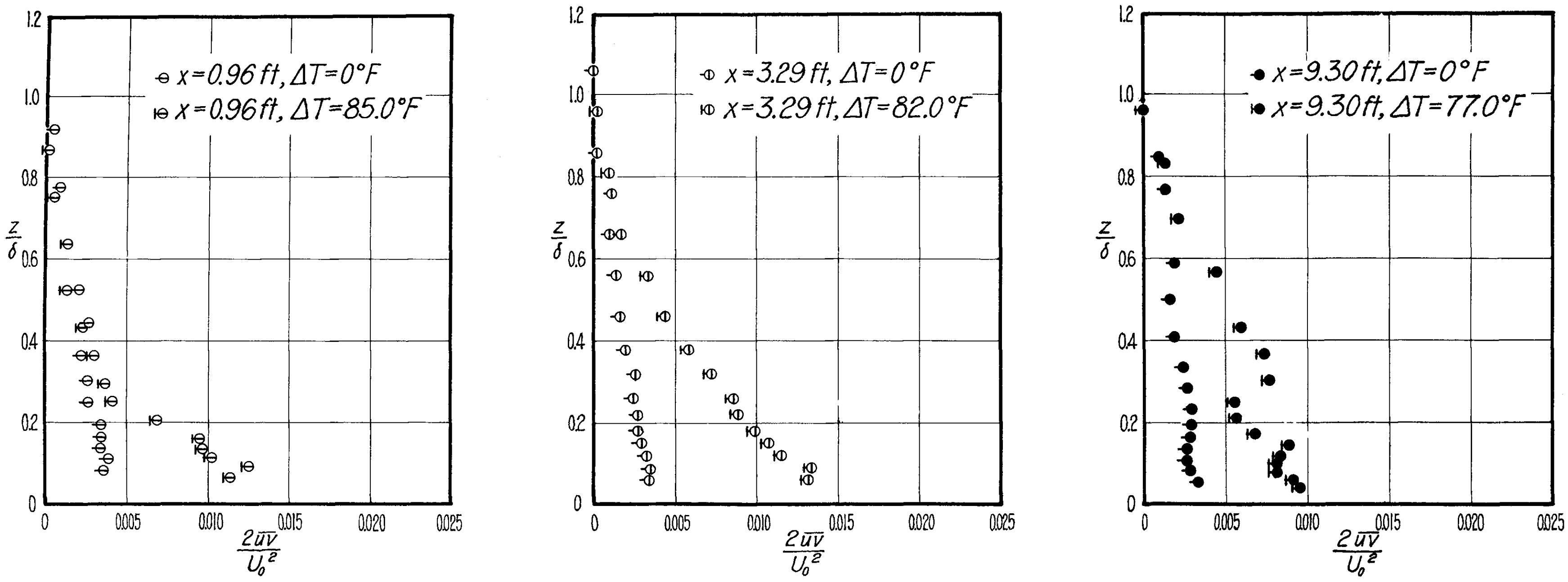

Fig. 18 Shear profiles for $U_0 = 17$ fps

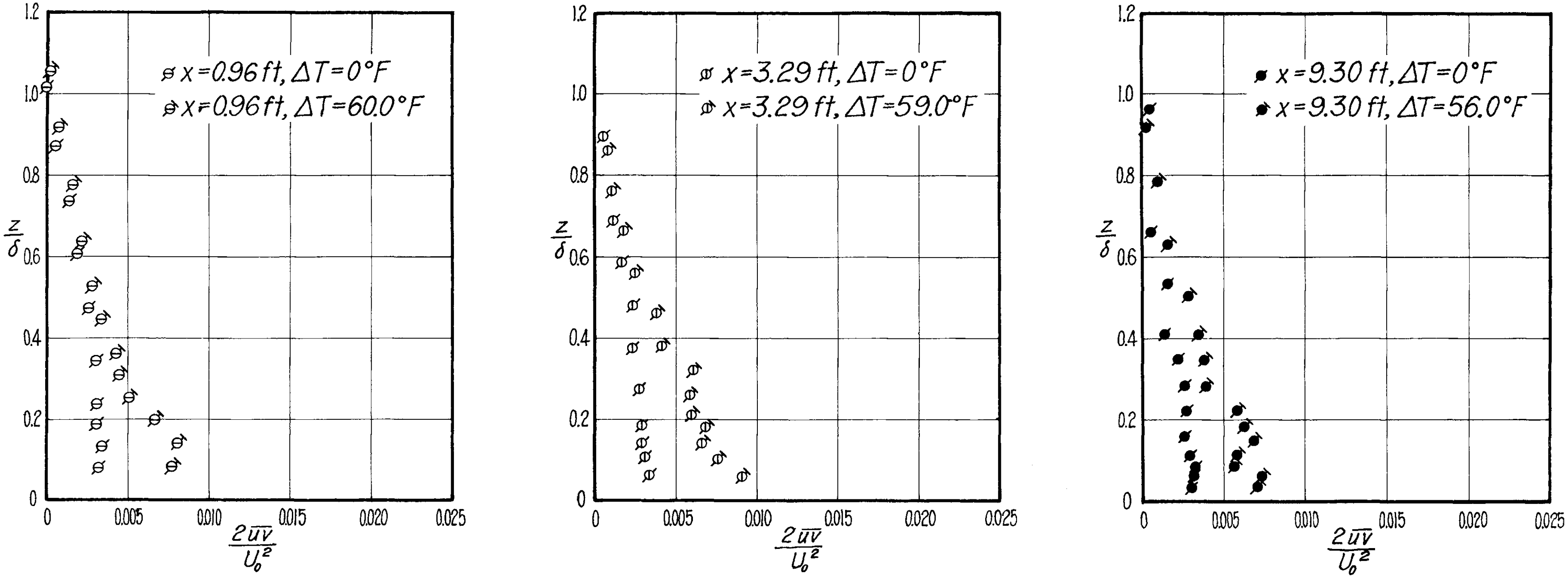

Fig. 19 Shear profiles for $U_0 = 35$ fps

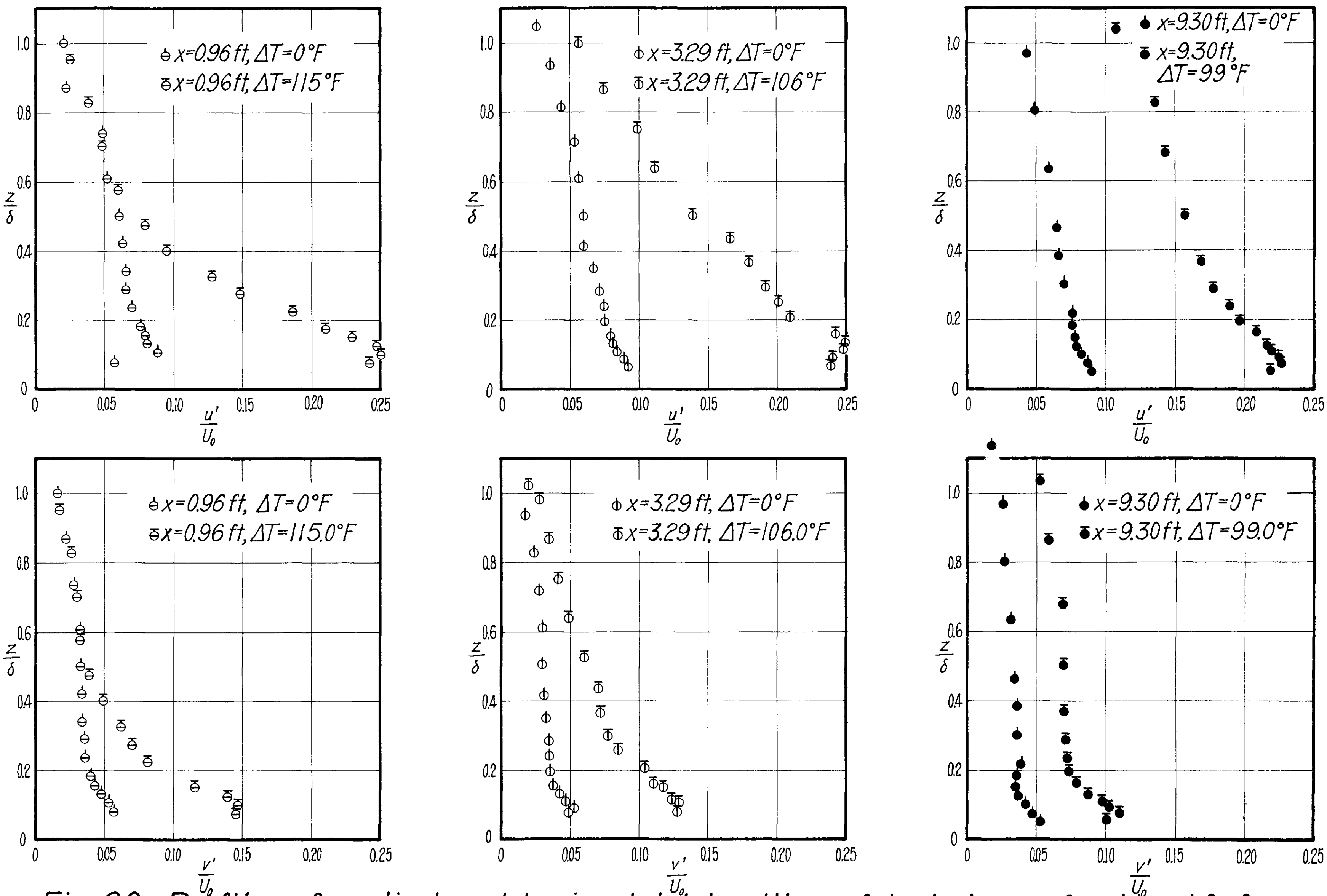

Fig. 20 Profiles of vertical and horizontal intensities of turbulence for $U_0 = 10$ fps

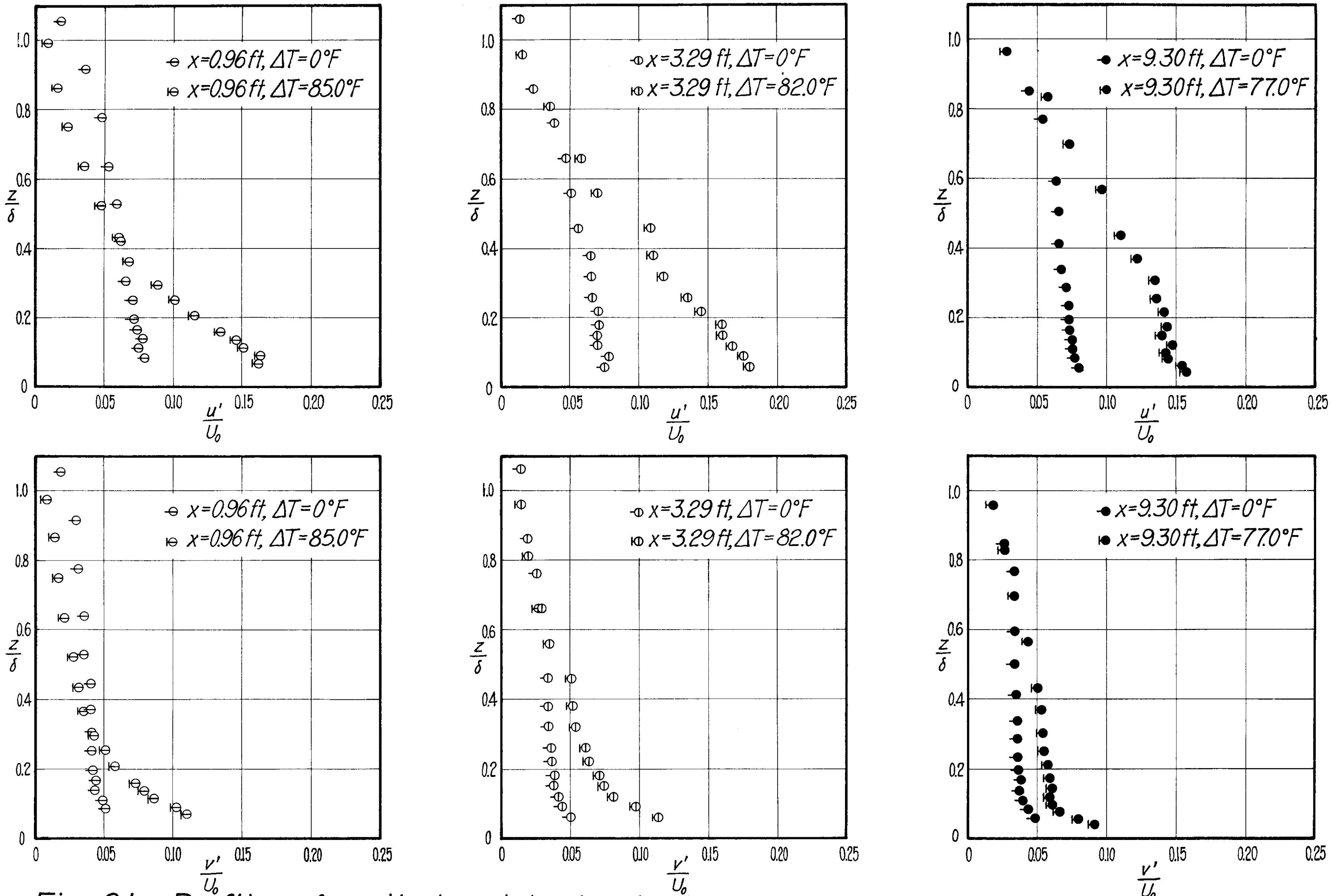

Fig. 21 Profiles of vertical and horizontal intensities of turbulence for $U_0 = 17$ fps

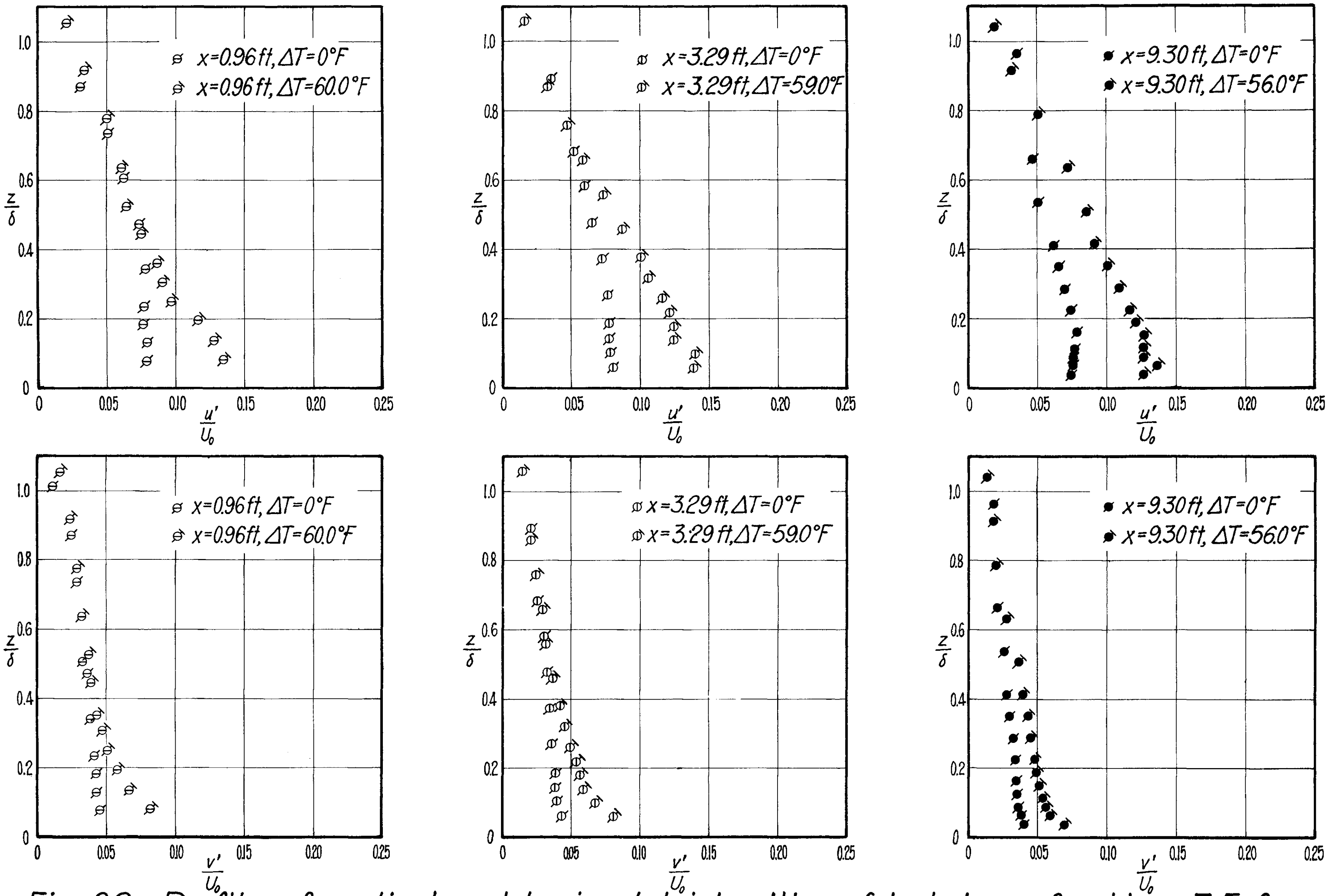

Fig. 22 Profiles of vertical and horizontal intensities of turbulence for $U_0 = 35$ fps

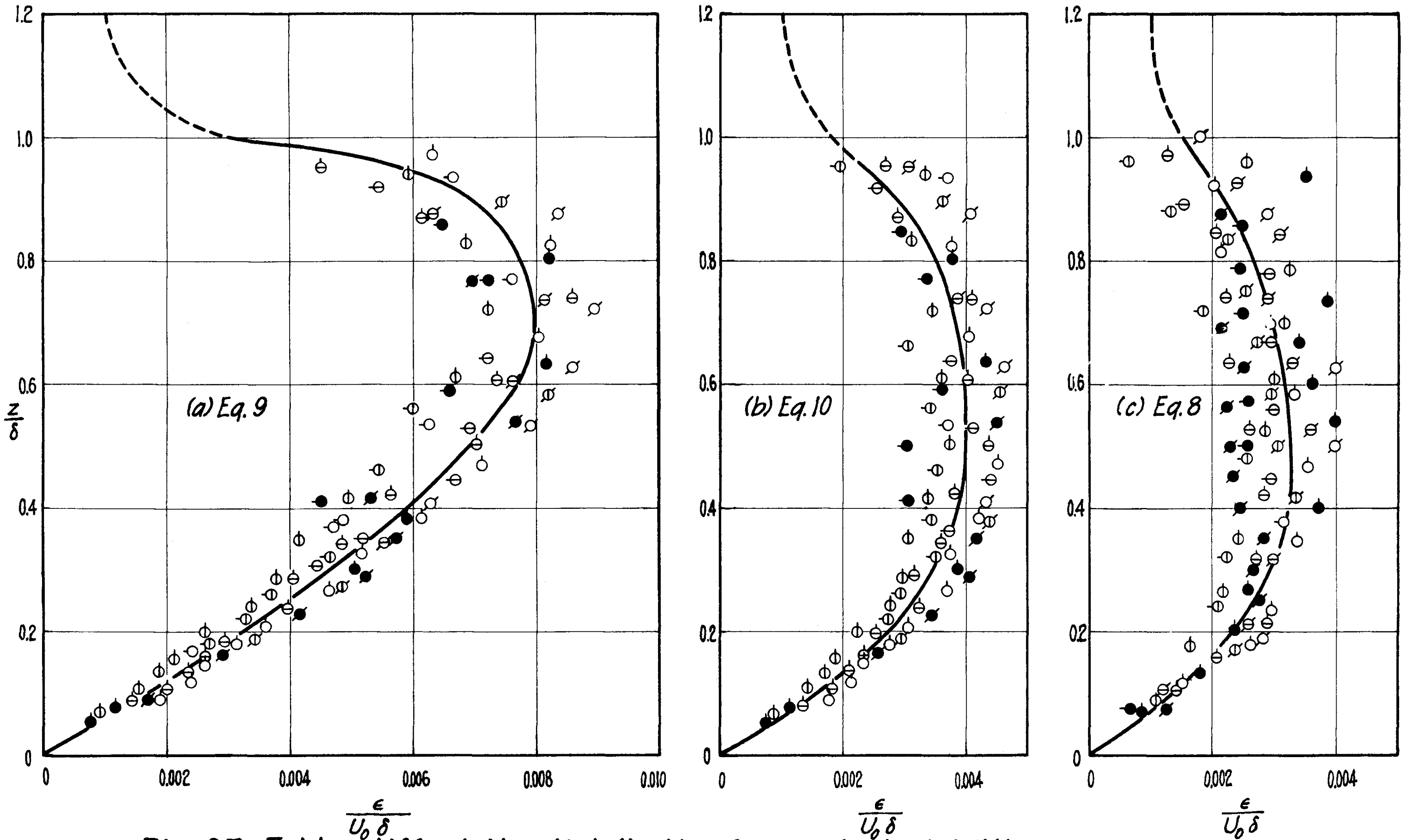

Fig. 23 Eddy diffusivity distribution for neutral stability:
(a) assuming logarithmic velocity distribution,
(b) assuming modified logarithmic velocity distribution, and
(c) numerical differentiation of the velocity profile as measured

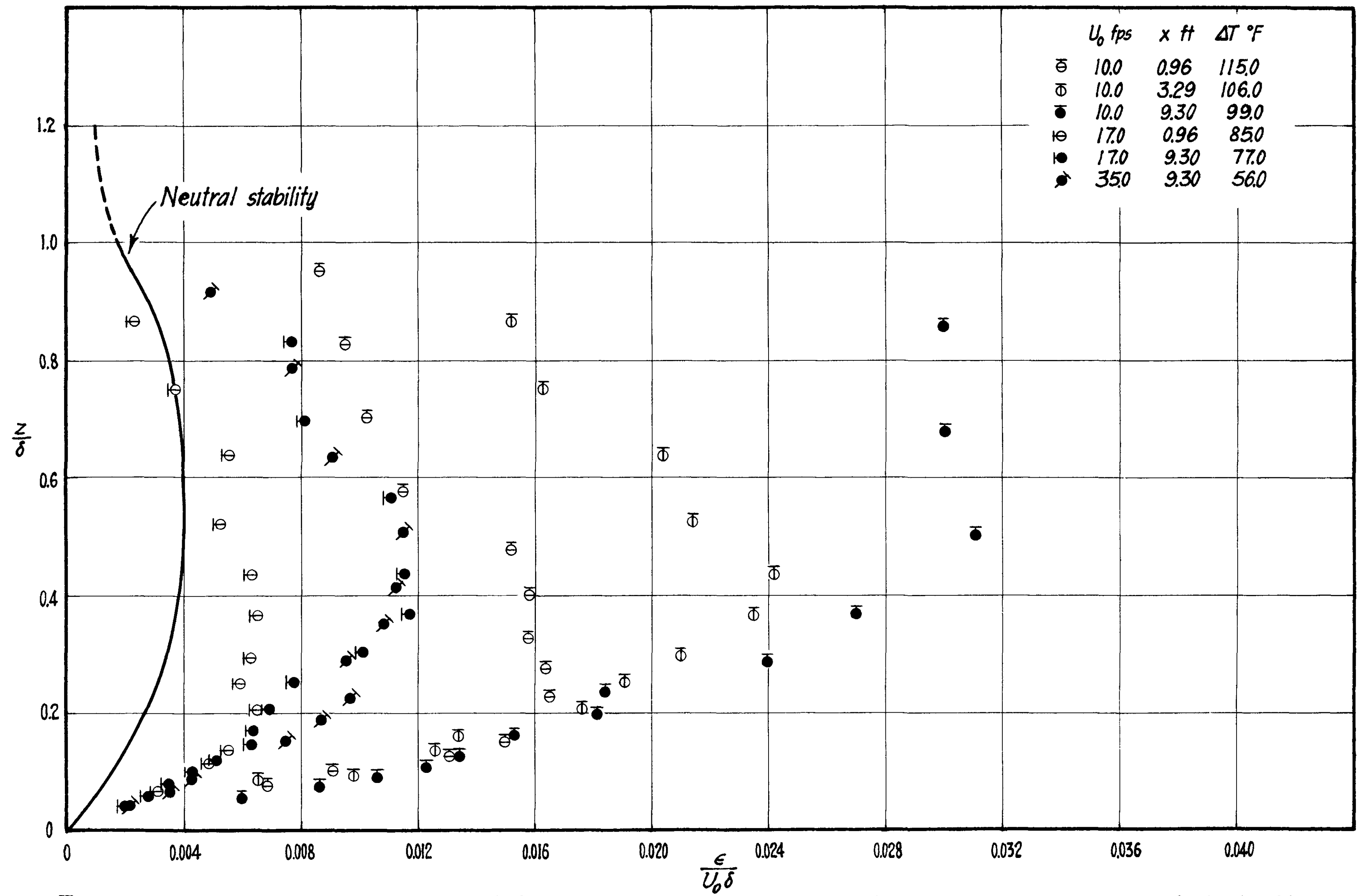

Fig. 24 Eddy diffusivity distributions assuming modified logarithmic velocity distribution

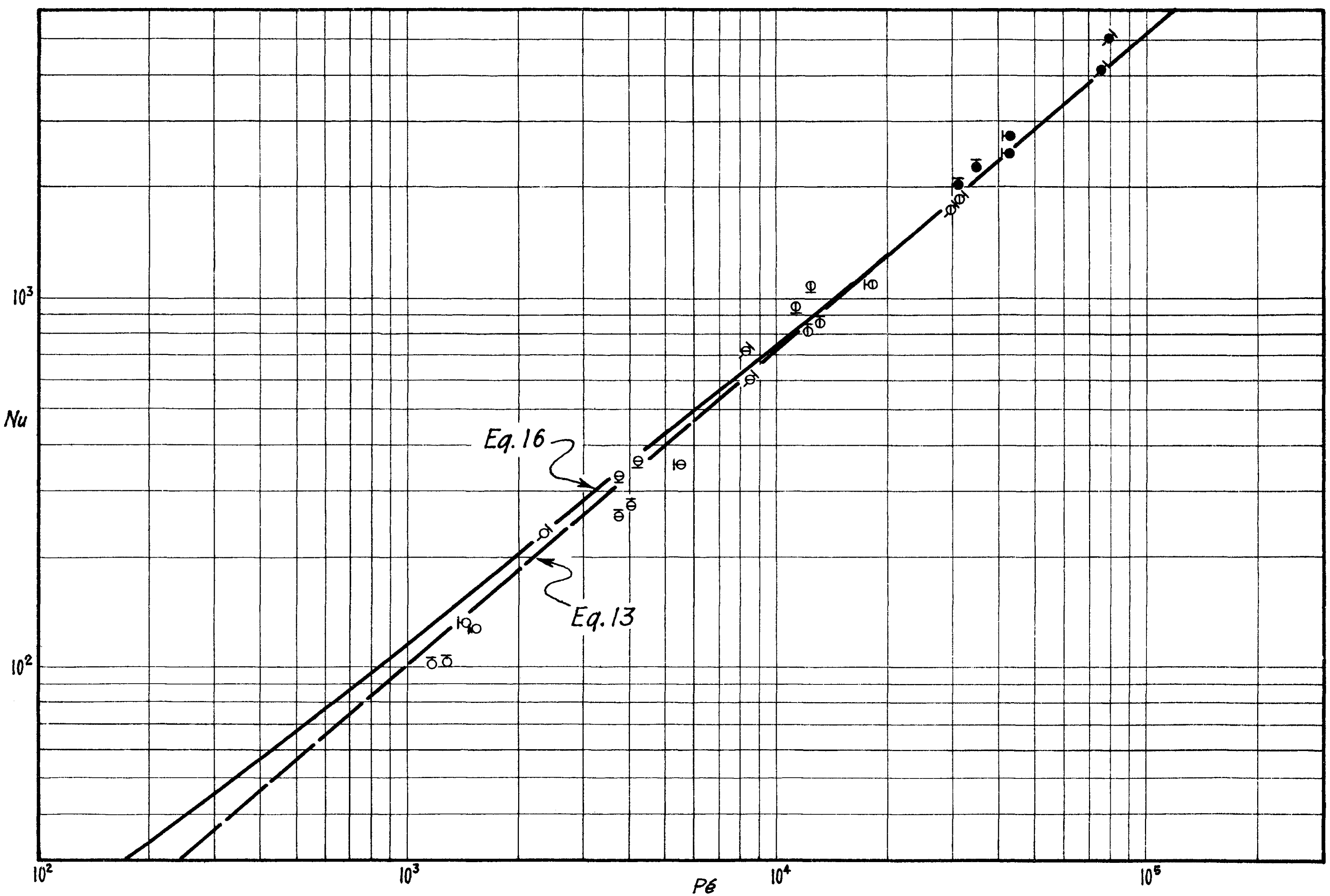

Fig. 25 Variation of Nusselt number with Peclet number

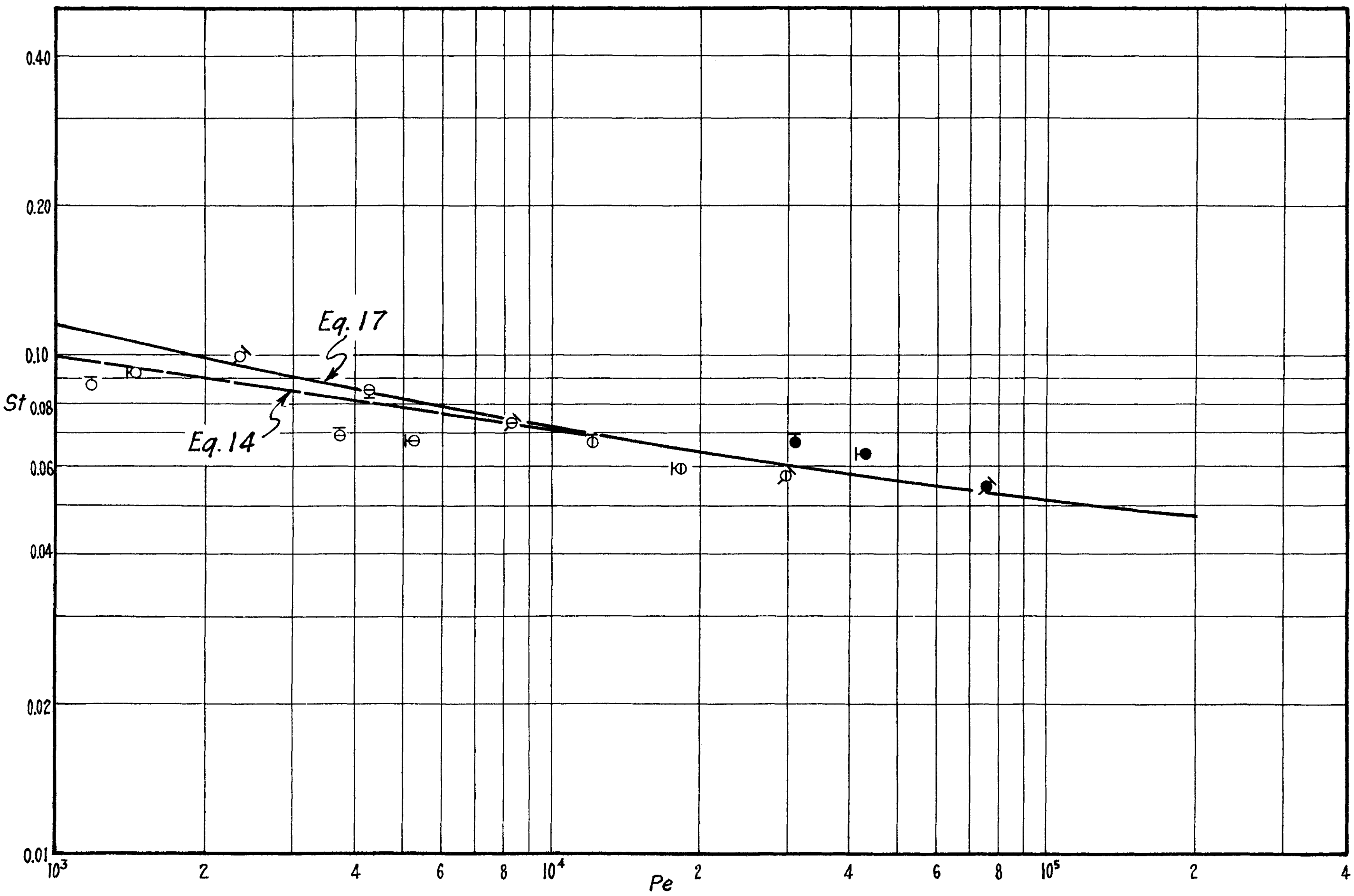

Fig. 26 Variation of Stanton number with Peclet number